



**HAL**  
open science

# Energy, exergy and exergoeconomic analysis and optimisation of the scale-up of a combined ammonia-water absorption pilot plant producing electricity and refrigeration

Simone Braccio, Hai Trieu Phan, Nicolas Tauveron, Nolwenn Le Pierrès,  
Alessia Arteconi

## ► To cite this version:

Simone Braccio, Hai Trieu Phan, Nicolas Tauveron, Nolwenn Le Pierrès, Alessia Arteconi. Energy, exergy and exergoeconomic analysis and optimisation of the scale-up of a combined ammonia-water absorption pilot plant producing electricity and refrigeration. *Energy Conversion and Management*, 2023, 278, pp.116686. 10.1016/j.enconman.2023.116686 . hal-03983508

**HAL Id: hal-03983508**

**<https://hal.science/hal-03983508>**

Submitted on 10 Feb 2023

**HAL** is a multi-disciplinary open access archive for the deposit and dissemination of scientific research documents, whether they are published or not. The documents may come from teaching and research institutions in France or abroad, or from public or private research centers.

L'archive ouverte pluridisciplinaire **HAL**, est destinée au dépôt et à la diffusion de documents scientifiques de niveau recherche, publiés ou non, émanant des établissements d'enseignement et de recherche français ou étrangers, des laboratoires publics ou privés.

# Energy, exergy and exergoeconomic analysis and optimisation of the scale-up of a combined ammonia-water absorption pilot plant producing electricity and refrigeration

Simone Braccio<sup>1,2,3</sup>, Hai Trieu Phan<sup>1</sup>, Nicolas Tauveron<sup>1</sup>, Nolwenn Le Pierrès<sup>2</sup>, Alessia Arteconi<sup>3,4,5,\*</sup>

<sup>1</sup> Univ. Grenoble Alpes, CEA, Liten, Campus Ines, 73375 Le Bourget du Lac, France

<sup>2</sup>LOCIE, Univ. Savoie Mont Blanc, CNRS UMR5271, Savoie Technolac, 73370 Le Bourget Du Lac, France

<sup>3</sup> Department of Mechanical Engineering, KU Leuven, 3000, Leuven, Belgium

<sup>4</sup> EnergyVille, 3600, Genk, Belgium

<sup>5</sup> Dipartimento di Ingegneria Industriale e Scienze Matematiche, Università Politecnica delle Marche, 60131, Ancona, Italy

\*Corresponding author: [simone.braccio@cea.fr](mailto:simone.braccio@cea.fr)

---

## ARTICLE INFO

## HIGHLIGHTS

### Keywords:

Combined absorption power-cooling cycle  
Exergy  
Exergoeconomic  
Low grade heat

- Thermodynamic and exergoeconomic assessment of a combined cooling and power cycle
- Study based on an existing ammonia water experimental prototype
- Scale-up of the considered plant predicted to reach exergy efficiency around 24%
- Unit cost of produced exergy of 28.31 \$/GJ obtained in the case of waste heat utilisation

---

## ABSTRACT

A low-temperature heat driven ammonia-water combined absorption cycle is studied in this paper from a thermodynamic and exergoeconomic point of view. The work is based on an absorption chiller prototype to which a partial admission turbine has been added in parallel to the cooling production line for the production of electricity.

First, the performance of the pilot plant is analysed in the design point and in a base case characterised by a hot source temperature of 100 °C, intermediate source temperature of 25 °C and cold source temperature of 10 °C. Exergoeconomic performance is assessed for two different cost of the fuel thermal input. Being the small scale of the plant very penalising, the scale-up of the plant to a size 25 times bigger is evaluated. Unit cost of products in this case is strongly reduced, mainly because of the constant cost and increased efficiency of the turbine.

Parametric studies are carried out on the temperature of the sources and on the size of components to assess how these parameters influence the performance of the cycle. Finally, an optimisation aiming at minimizing the unit cost of products is performed on the size of heat exchangers for the base case working point and fixing constant the size of the turbine. The optimised cycle layout allows reaching a unit cost of produced cooling of 10.14 \$/GJ (0.036 \$/kWh) and a cost of produced electricity of 40.45 \$/GJ (0.145 \$/kWh) if the cost of the thermal input is neglected. When a thermal input cost of 15 \$/GJ is considered, the calculated cooling and electricity cost are 66.7 \$/GJ (0.24 \$/kWh) and 106.8 \$/GJ (0.384 \$/kWh) respectively. In both cases the optimal vapour split ratio between cooling and power production lines is found to be around 0.47.

---

## 1. Introduction

In recent decades, a growing attention has been paid by the international community to environmental issues and climate change. Concerns extend to all sectors, including the production of cooling and electricity. Increase of the population and development of the global economy have driven a steep increase in space-cooling needs: worldwide demand in 2016 tripled with respect to 1990 values and is expected to further triple between 2016 and 2050 [1]. In these circumstances, the use of cooling technologies activated by low grade heat has attracted great interest [2][3]. In particular, thermodynamic cycles enable a cost effective and proven way to convert heat into cooling. Thermally driven cooling systems include absorption[4], adsorption[5], desiccant systems using solids [6] and liquids [7], ejector-compression systems [8] and hybrid systems [9].

These systems consume very little electricity resulting in fewer climate-changing gas emissions and therefore their increased adoption is a key to improve the sustainability of cooling.

Absorption systems [4] are very well suited for the recovery of thermal energy as they replace the mechanical vapour compression of standard air conditioners by thermochemical compression. The circulation pump in such

systems consumes a modest amount of electricity and they can use any type of thermal source as the main driver, in particular renewable sources (e.g. solar) or waste heat.

Nomenclature			Subscripts and superscripts	
<i>Letter symbols</i>			<i>a</i>	absorber
<i>A</i>	section	[m <sup>2</sup> ]	<i>c</i>	condenser
<i>c</i>	cost per unity of exergy	[\$.] <sup>-1</sup>	<i>cooling</i>	cooling
<i>C</i>	absolute velocity	[m. s <sup>-1</sup> ]	<i>CH</i>	chemical
$\dot{C}$	cost rate	[\$.s <sup>-1</sup> ]	<i>CI</i>	capital investment
<i>cp</i>	heat capacity	[W.m <sup>-2</sup> K <sup>-1</sup> ]	<i>cv</i>	control volume
<i>ex</i>	specific exergy	[J.kg <sup>-1</sup> ]	<i>d</i>	desorber
$\dot{E}x$	exergy flow rate	[W]	<i>D</i>	destroyed
<i>f</i>	exergoeconomic factor	[-]	<i>e</i>	evaporator, energy
<i>h</i>	specific enthalpy	[J.kg <sup>-1</sup> ]	<i>eff</i>	effective
<i>i<sub>r</sub></i>	interest rate	[-]	<i>ele</i>	electric
<i>Ja</i>	Jakob number	[-]	<i>ex</i>	exergetic
<i>k</i>	constant, component		<i>F</i>	fuel
<i>K</i>	overall heat transfer coefficient	[W.m <sup>-2</sup> K <sup>-1</sup> ]	<i>fr</i>	friction
<i>L</i>	latent heat	[J.kg <sup>-1</sup> ]	<i>gen</i>	generator
<i>M</i>	molar mass	[kg.mol <sup>-1</sup> ]	<i>id</i>	ideal
$\dot{m}$	mass flow rate	[kg.s <sup>-1</sup> ]	<i>i</i>	inlet
<i>n</i>	system lifetime	[years]	<i>is</i>	isentropic
<i>P</i>	pressure	[P]	<i>I</i>	first principle
$\dot{Q}$	thermal power	[W]	<i>KN</i>	kinetic
<i>R</i>	ideal gas constant	[J. K <sup>-1</sup> mol <sup>-1</sup> ]	<i>L</i>	loss
<i>R<sub>en</sub></i>	energetic ratio	[-]	<i>lk</i>	leaking
<i>r<sub>s</sub></i>	split ratio	[-]	<i>lm</i>	logarithmic mean
<i>s</i>	specific entropy	[J. K <sup>-1</sup> . kg <sup>-1</sup> ]	<i>LF</i>	limiting fluid
<i>S</i>	heat exchangers area	[m <sup>2</sup> ]	<i>liq</i>	liquid
<i>T</i>	temperature	[K]	<i>max</i>	maximum
<i>U</i>	rotational speed	[m. s <sup>-1</sup> ]	<i>mech</i>	mechanical
<i>W</i>	specific work	[J.kg <sup>-1</sup> ]	<i>min</i>	minimum
$\dot{W}$	mechanical/electrical power	[W]	<i>net</i>	net
<i>x</i>	ammonia mass fraction	[-]	<i>NLF</i>	non-limiting fluid
$\gamma$	rate of exergy destruction (loss )	[-]	<i>o</i>	outlet
	to total fuel exergy		<i>OM</i>	operating and maintenance
$\gamma^*$	rate of exergy destruction (loss )	[-]	<i>p</i>	pump
	to total exergy destruction		<i>P</i>	product
<i>Z</i>	capital cost	[\$]	<i>pa</i>	partial admission
$\dot{Z}$	capital cost rate	[\$.s <sup>-1</sup> ]	<i>pass</i>	passage
<i>Greek letters</i>			<i>PH</i>	physical
$\gamma$	maintenance factor	[-]	<i>prod</i>	products
$\gamma_a$	adiabatic index	[-]	<i>PT</i>	potential
$\Delta$	variation		<i>Q</i>	thermal
$\epsilon$	heat exchangers effectiveness	[-]	<i>refvalv</i>	refrigerant throttling valve
$\eta$	efficiency	[-]	<i>sat</i>	saturated
$\omega$	rotational speed	[rpm]	<i>shx</i>	solution heat exchanger
$\rho$	density	[kg.m <sup>-3</sup> ]	<i>sol</i>	solution
$\tau$	operating hours	[h]	<i>solvalv</i>	solution throttling valve
<i>Acronyms</i>			<i>species</i>	species
APC	absorption power and cooling		<i>sub</i>	subcooler
CEPCI	chemical engineering plant cost index		<i>sh</i>	superheater
COP	coefficient of performance		<i>t</i>	turbine
CRF	capital recovery factor		<i>th</i>	thermal
H <sub>2</sub> O	water		<i>throat</i>	throat
HTF	heat transfer fluid		<i>tot</i>	total conditions
NH <sub>3</sub>	ammonia		<i>u</i>	tangential
NTU	number of transfer units		<i>vap</i>	vapour
ORC	organic Rankine cycles		<i>w</i>	work
O&M	operating and management		<i>0</i>	reference state
SI	international system		<i>1,2,...</i>	system state points
UCOPE	unit cost of produced exergy	[\$.G] <sup>-1</sup>		

Research has focused on improving the performance of thermal cooling systems by combining power cycles, such as the Kalina cycle [10] or the Rankine cycle [11], with absorption cycles (APC) to produce both cooling and power using only one heat source rather than coupling two cycles in cascade. This can lead to an increased system

efficiency and more effective usage of the heat source [12], as well as the mutualisation of components for vapour generation, condensation, pumping, etc.

The most commonly used absorbent-absorbate working pair in APC cycles is ammonia-water ( $\text{NH}_3\text{-H}_2\text{O}$ ) [13]. This working pair has several advantages including very good thermophysical properties (e.g. ammonia's very high latent heat of 1226 kJ/kg [8] leading to compact machines), no crystallization, broad operation range and possibility to reach sub-zero temperatures [14]. Ammonia is a natural fluid not harmful to the environment [15], having a global warming and an ozone depletion potential of zero [8]. Furthermore, the use of binary mixtures, recently practised also in ORCs [16], has been reported to achieve high conversion efficiencies [17] thanks to an improved thermal matching with heat sources and sinks, reducing exergetic losses with respect to traditional heat exchange processes [18].

Two main types of architectures are distinguished in literature: series [19][20] and parallel [21][22] architectures. The former generally privilege the production of electricity while the latter offer more flexibility between the two production modes. More details regarding the two architectures are given by Ayou et al. [13].

Goswami et al. [23] proposed the first combined dual pressure power and cooling cycle combining a Rankine cycle and an absorption refrigeration cycle in series. Hasan et al. [24] performed the optimization of the same cycle from the perspective of the second law of thermodynamics. The authors obtained a maximum second law efficiency of 65.8% at 147 °C heat source temperature while the maximum irreversibility was found to take place in the absorber (44% of total irreversibility) with the rectifier and the solution heat exchanger also contributing significantly (16% and 24% respectively). Zare et al. [25] conducted a thermoeconomic optimization of the Goswami cycle obtaining a 18.6% and 25.9% reduction in the sum of the unit cost of the system products compared to the cost of the cycle products obtained through at the cycle optimized from the first and second law of thermodynamics viewpoint respectively.

Zhang et al. [26] studied the possibility of producing refrigeration and power by arranging a Rankine cycle in parallel with an absorption refrigeration cycle. The cycle had a good thermal performance, with energy and exergy efficiencies of 27.7% and 55.7%, respectively, for the base-case studied (having a maximum cycle temperature of 450°C). Wang et al. [22] proposed a new combined power and ejector-absorption refrigeration cycle combining the Rankine cycle and the ejector-absorption refrigeration cycle, to produce both power and refrigeration output simultaneously. The introduction of an ejector between the rectifier and the condenser, provided a performance improvement without greatly increasing the complexity of the system. For 25 bar pressure and 285 °C temperature at inlet of the turbine and 1.2 bar pressure and 96 °C temperature at the exit of the turbine, thermal and exergy efficiencies of the system were 20.97% and 35.77% respectively.

Sun et al. [27] investigated an ammonia-water based system for power and cooling cogeneration using mid/low temperature heat source in which the high-temperature portion of waste heat is used for power generation, whereas the low-temperature part is used for refrigeration. In addition, the exhaust heat of the power subsystem is recovered by the refrigeration subsystem. Compared with separate power and refrigeration systems, the proposed system consumed 17.1% less heat with the same output.

Mendoza et al. [28] focused their research on the integration of a scroll expander in an absorption cycle in parallel to the refrigeration line for the simultaneous production of cooling and power. Parametric cycle study was performed using three different working fluids,  $\text{LiNO}_3$ ,  $\text{NaSCN}$  and ammonia-water, showing that exergy efficiency and first law efficiency (43% and 11% respectively) decrease when increasing the power production of the cycle. Villada et al. [29] compared the Goswami cycle with the parallel single-stage combined absorption cycles studied by Mendoza. It was concluded that, if the main objective is the power production, the Goswami cycle offers the best first and second law efficiencies, while, if the main interest is the production of cooling, parallel architectures are the best option despite relatively lower efficiencies.

Mohmoudi and Kordlar [30] proposed the combination of a Kalina cycle with a double effect absorption cycle for harvesting geothermal energy. The cycle was optimized for both maximum exergy efficiency and minimum total product cost showing that in the second case the total product unit cost is around 17% lower than in the first, with a highest exergy efficiency found of 34.8% and minimum cost of products obtained of 24.5 \$/GJ respectively. The same authors performed an exergoeconomic analysis of the combination of an absorption chiller and an organic Rankine cycle showing that designing the cycle to achieve minimum total product unit cost resulted in total product unit cost 20.4% and 24.3% lower than one maximising first law and second law efficiency respectively. Results also indicated that priority components for modification were the turbine, condenser and absorber.

Shokati et al. [31] investigated two different configurations of a double effect absorption refrigeration/Kalina cogeneration cycle for the recovery of heat from high temperature heat sources. Seyfour [32] analysed a

cogeneration system consisting of an organic Rankine cycle and a hybrid GAX cycle using geothermal hot water at 133 °C to produce power and cooling at -50 °C. A maximum exergy efficiency of 42.8% with a total unit product cost of 4.19 \$/GJ was obtained.

The above review highlights the interest of combining cooling and power generation systems. However, it should be noted that the performance of these systems still needs to be improved as they often remain bulky, heavy and more costly than conventional systems [33]. Exergoeconomics (also known as thermoeconomic), combining thermodynamic analysis with economic analysis [34], has emerged in this respect, as one of the best scrutinizing tools to assess and optimise the performance of these cycles for a given application.

While several exergoeconomic analyses have been performed on combined power and cooling cycles, most of them are generally limited to high heat source temperatures [31][35] or complex architectures [36]. The present work investigates a low-temperature heat driven absorption cooling and power (APC) production system with a parallel architecture, using the ammonia-water mixture, with a focus on space cooling (around 10 °C).

The originality of the study is threefold. First, the work is based on an existing absorption combined cooling and power pilot plant [37] characterised by the presence of novel combined desorber and a partial admission impulse turbine. The combined desorber allows both the desorption and purification of the ammonia vapour, thus avoiding the need of a separated rectifier and simplifying the architecture of the cycle. On the other hand, the micro-turbine allows to produce electrical power also at the prototype scale.

The second novelty is related to the modelling of the components: unlike most similar available studies from literature which are based on simplified representations of heat exchangers and turbine (e.g. fixed heat exchangers temperature pinches and isentropic turbine efficiency), in this work detailed physical models of the components adjusted on experimental data from the prototype are used. Finally, feedback and experimental data from the pilot plant allowed access to accurate data concerning components cost.

The prototype set-up and the previously developed absorption chiller [38] and turbine [39] models are described briefly in **Section** Erreur ! Source du renvoi introuvable.. Subsequently, the energy and exergy performance of the pilot plant is analysed through parametric studies and exergoeconomic parameters are evaluated based on the methodology detailed in [34]. An exergoeconomic analysis of the combined plant is then performed with the objective of understanding the cost formation process within the plant and how costs can be divided between the two products: cooling and power output. An evaluation of the scale-up of the plant is carried out for a base case working point, representative of a refrigeration application, to assess economic attractiveness of the application and thermodynamic and exergoeconomic performance change with plant size.

Finally, fixing the size of the turbine and the solution mass flow rate, an optimisation of the heat exchangers area is carried out for the scaled-up plant working in the base case conditions to minimize the unit cost of exergy of the products.

## 2. Description of the cycle

### 2.1. Cycle architecture

The APC cycle under investigation is shown schematically in **Fig. 1**. The functioning is based on an ammonia-water absorption machine with an expander coupled in parallel to the cold production circuit. The ammonia rich liquid solution at the absorber outlet (point 1) is pumped into the desorber where a supply of thermal power  $\dot{Q}_d$  allows the partial desorption of ammonia vapour. It should be noted that the hot temperature heat transfer fluid is firstly used to superheat the vapour entering the turbine and then to supply power to the desorber.

A second line comprising an expansion valve returns the poor solution to the absorber. The solution heat exchanger preheats the rich solution before it enters the desorber. The refrigerant vapour (almost pure in ammonia) produced at the desorber (point 7) is divided between the cooling (point 8) and the electricity production lines (point 14).

On the electricity production line, a superheater increases the vapour temperature before it enters the turbine in order to avoid condensation during expansion and increase the mechanical power production efficiency. The superheated steam enters the turbine where mechanical work is produced.

On the cold production line, the refrigerant vapour condenses through the exchange of thermal power with an intermediate temperature source. Before cooling the cold source at the evaporator, the fluid is expanded in a valve to reach the low pressure. A sub-cooler is used to pre-cool the refrigerant before it expands using the fluid coming out from the evaporator. The flows of the cooling (point 13) and electrical power production lines (point 16) mix

and are finally absorbed in the poor solution through cooling by an intermediate temperature source (generally the same used in the condenser).

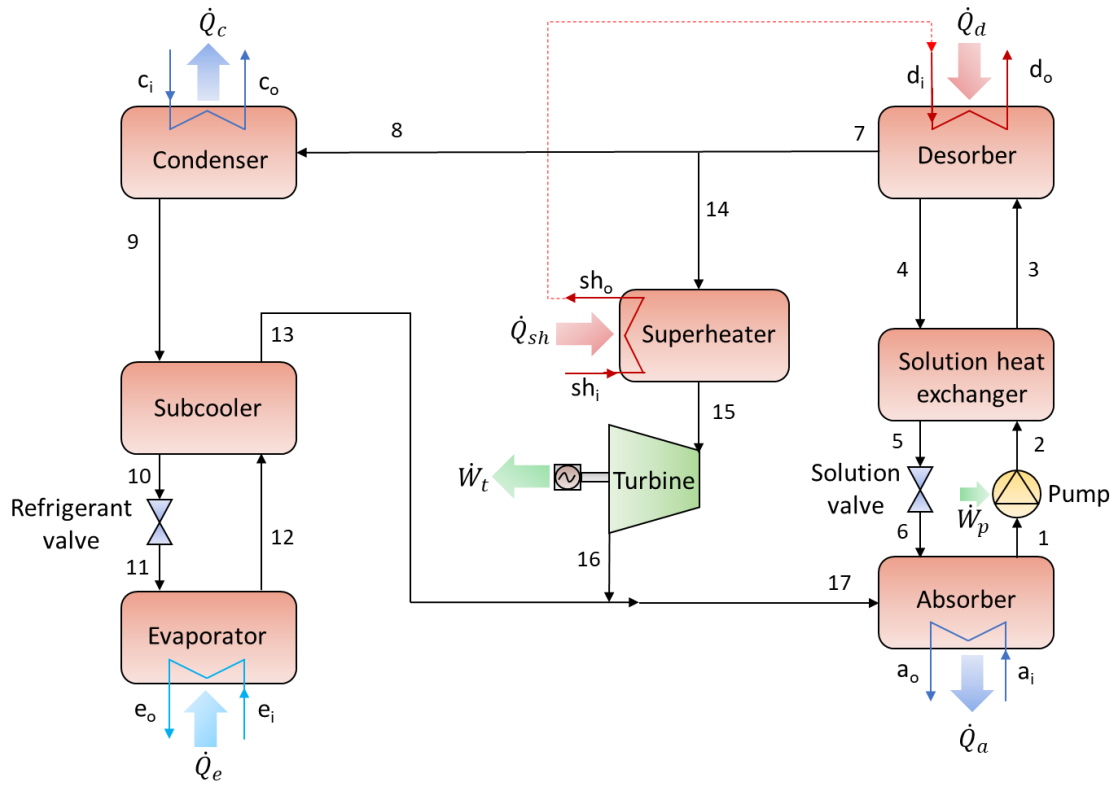


**Fig. 1.** Schematic of the combined cooling and power (APC) cycle.

## 2.2. Experimental pilot plant

The study is based on an existing absorption chiller device developed at CEA INES [38]. The prototype (shown in **Fig. 2**) is a thermally driven single-effect ammonia-water absorption chiller of 7 kW cooling capacity designed for solar cooling applications with the goal of testing innovative architectures [40].

The chiller is composed of six plate falling-film heat exchangers, the four main ones being external heat and mass exchangers: desorber, absorber, evaporator and condenser. The others are two internal heat exchangers needed to improve the performance of the cycle: the solution heat exchanger and the subcooler.

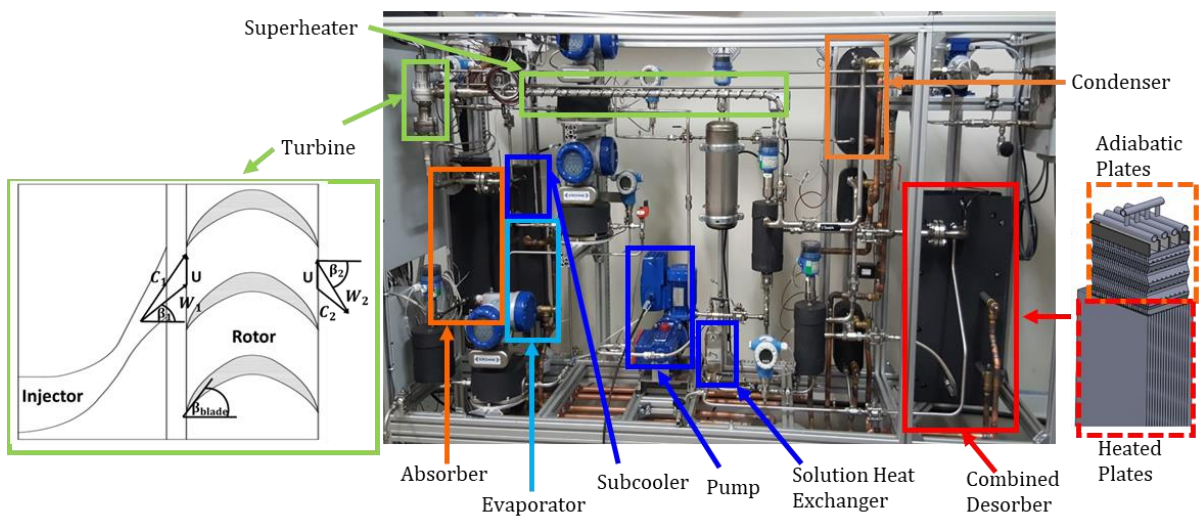


**Fig. 2.** Picture of the prototype of the  $\text{NH}_3/\text{H}_2\text{O}$  combined cycle with a focus on key components: turbine (left) and combined desorber (right).

The desorber, a newly developed combined component [41] is also based on the falling film technology. This heat exchanger (right side of **Fig. 2**) is composed of a lower part where vapour is generated exchanging heat with the hot source, and an adiabatic upper part which purifies the desorbed vapour by partial reabsorption of the water in the ammonia-water solution entering the exchanger. The combination of the heated and adiabatic sections makes it possible to replace two plate heat exchangers used for the desorber and the rectifier as well as two associated phase-separation bottles with only one component, thus helping to reduce costs and overall dimensions [42].

The temperatures and the mass flow rates of the HTFs (the external heat transfer fluids) and the rich solution mass flow rate are the only available control parameters of the pilot plant [38]. The design values and variability range for these parameters are shown **Table 1**.

**Table 1.** Design values for components of the absorption machine. Inlet/outlet values are shown for heat exchangers HTF temperatures.

		Evaporator	Condenser	Absorber	Desorber
Temperature [°C]	Nominal	18/13	27/32	27/32	95/90
	Minimal	10/5	23/28	23/28	85/80
	Maximal	22/17	31/36	31/36	106/101
Pressure [bar]	Nominal	7	12	7	12
	Minimal	5	11	5	11
	Maximal	8	14	8	14
HTF Mass flow rate [kg/h]	Nominal	1100	1200	1200	1600
Power [kW]	Nominal	7	7	9	10

The geometry of the stainless steel corrugated heat exchangers of the cycle is given in **Table 2**. As shown, the surface of the adiabatic upper part allowing the purification of the vapour is about 35 % of the surface of the vapour generating lower part (exchanging heat with the hot source).

**Table 2.** Dimensions of the heat exchangers of the cycle.

	Absorber	Condenser	Desorber heated (adiabatic) part	Evaporator	Solution Heat Exchanger	Subcooler
Plate width [mm]	96	111	320 (100)	111	72	72
Plate length [mm]	668	310	150 (90)	310	187	187
Plate thickness [mm]	0.5	0.5	6 (0.8)	0.5	0.5	0.5
Number of plates [-]	16	40	16 (28)	24	25	20
Total surface [m <sup>2</sup> ]	0.89	1.30	0.67 (0.23)	0.75	0.31	0.24

The integration in the loop of an expander was investigated for the production of electricity [39]. Given the small ammonia mass flow rate involved (around 20 kg/h) and the limited pressure drop available, the expander selection process leads to the choice of a partial admission axial turbine.

The schematic diagram of the partial admission supersonic impulse axial turbine is shown on the left side of **Fig. 2**. The turbine, designed for an inlet pressure of 16 bar and an outlet pressure of 4 bar, is characterised by 27 rotor blades but a distributor composed of a single converging-diverging injector. The choice of a partial admission expander allows avoiding excessively small and unfeasible dimensions or too high and impracticable rotational speed at the cost of increased partial admission losses.

The electricity production line is completed by the presence of a superheater of a maximal power of 1 kW. It should be noted that, since the vapour is cooled and purified by the rich solution in the adiabatic part of the desorber (**Fig. 2**), its temperature at outlet ( $T_7$ ) is close to that of the solution at inlet ( $T_3$ ). The goal of the superheater is hence to superheat the vapour up to the hot source temperature.

### 3. Thermodynamic analysis

#### 3.1. Numerical model of the cycle

A numerical model of the absorption cycle previously introduced was developed in EES (Engineering Equation Solver) and adjusted on experimental results as detailed in a previous work [38]. The correlations proposed by Ibrahim and Klein [43] were used to calculate the thermodynamic properties of the ammonia-water mixture because of their good agreement with experimental data. For each component, the energy and mass conservation equations were formulated in the steady state assumption based on the description in [4]. It is assumed that the mixture is saturated at the outlet of condenser and desorber. Considering the specificity of the desorber presented previously, in ideal conditions, the refrigerant vapour at outlet reaches the same temperature as the solution at the inlet and its concentration is that of saturated vapour at the inlet temperature of the rich solution  $T_3$ . The conditions of the poor solution at the outlet can then be calculated through an energy balance on the desorber [38].

The isentropic efficiency of the pump was considered equal to 80% [37], expansions in valves are considered isenthalpic and pressure drops as well as thermal losses are neglected.

Each exchanger of the absorption chiller was experimentally characterised using either an efficiency or a temperature pinch with respect to the HTF, comparing the actual performance of exchangers with that of ideal components. These parameters were modelled using three dimensionless numbers: the energetic ratio  $R_{en}$ , the number of transfer units  $NTU$  and the Jakob number  $Ja$  as detailed in [38].  $R_{en}$  is defined as the ratio of the maximum power transferable to the non-limiting fluid over the maximum power transferable to the limiting fluid in the exchange:

$$R_{en} = \frac{\dot{Q}_{NLF,max}}{\dot{Q}_{LF,max}} \quad (1)$$

The number of transfer units  $NTU$  is a dimensionless parameter characterizing the rate of heat transfer in counter-current exchangers. It is defined as the ratio of the product of the heat transfer coefficient  $K$  and the exchange  $S$  surface to the smallest heat capacity rate between the two fluids [44]:

$$NTU = \frac{K \cdot S}{(\dot{m} \cdot c_p)_{min}} \quad (2)$$

The global heat transfer coefficient  $K$  considers both convective transfers between falling film and plate and between the HTF and plate and conduction across the absorber plate. The HTF side heat transfer coefficient is calculated with a correlation developed for corrugated plates with a Reynolds number value between 50 and 14,600 [45], while the convective heat transfer coefficient between the falling film and the cooling plates is calculated with the Wilke's correlation [46].

The Jakob number ( $Ja$ ) is a dimensionless number defined here as the ratio of the solution sensible heat to the latent heat released during the liquid vapour phase change:

$$Ja = \frac{\rho_{sol} \cdot c_{p,sol} \cdot (T_{HTF,i} - T_{liq,sat})}{\rho_{vap} \cdot L} \quad (3)$$

Where  $\rho_{sol}$ ,  $c_{p,sol}$  and  $L$  are the density, specific heat and latent heat of vaporization of the entering solution,  $T_{HTF,i}$  is the temperature of the HTF at inlet and  $T_{liq,sat}$  is the temperature of the saturated liquid at the inlet at the given pressure and concentration. **Table 3** shows the semi-empirical correlations used to model each effectiveness.

**Table 3.** Effectiveness and temperature pinch correlation used for each component.

Component	Effectiveness	Correlation
Absorber	Thermal effectiveness	$\varepsilon_{th,a} = 1 - \exp(-9.2 \cdot 10^{-3} \cdot Ja_a^{0.4} \cdot NTU_a^{1.5} \cdot R_{en,a}^{-0.72})$
	Mass effectiveness	$\varepsilon_{mass,a} = 1 - \exp(-9.1 \cdot 10^{-4} \cdot Ja_a^{0.4} \cdot NTU_a^{1.5} \cdot R_{en,a}^{-0.92})$
Condenser	Temperature pinch	$\Delta T_c = (T_8 - T_{ci}) \cdot \exp(-6.2 \cdot 10^{-1} \cdot NTU_c^{0.2} \cdot R_{en,c}^{0.3})$
Desorber	Thermal effectiveness	$\varepsilon_{th,d} = 1 - \exp(-6.0 \cdot 10^{-3} \cdot Ja_d^{1.3} \cdot NTU_d^{1.5} \cdot R_{en,d}^{0.5})$
	Species effectiveness	$\varepsilon_{species,d} = 1 - \exp(-2.3 \cdot 10^{-1} \cdot Ja_d^{1.3} \cdot NTU_d^{-0.5} \cdot R_{en,d}^{0.3})$
Evaporator	Temperature pinch	$\Delta T_e = (T_{ei} - T_{11}) \cdot \exp(-7.2 \cdot 10^{-2} \cdot NTU_e^{0.7} \cdot R_{en,e}^1)$
Solution heat exchanger	Thermal effectiveness	$\varepsilon_{th,shx} = 1 - \exp(-6.3 \cdot 10^{-1} \cdot NTU_{shx}^{0.88} \cdot R_{en,shx}^{0.5})$
Subcooler	Thermal effectiveness	$\varepsilon_{th,sub} = 1 - \exp(-5.4 \cdot 10^{-2} \cdot NTU_{sub}^{1.8} \cdot R_{en,sub}^{2.2})$

Thermal effectiveness measures the ratio of power exchanged by the component to the power exchanged by an ideal component. Mass effectiveness is the ratio of absorbed vapour with respect to the vapour mass flow rate

absorbed by an ideal absorber. Species effectiveness measures the purity of the ammonia vapour with respect to the maximum purity attainable with an ideal combined desorber.

Results of the model show very good agreement with experimental, with an average error of 2.4% and 5.4% for the predicted COP and cooling power output respectively (Table 6 in reference [38]).

The model developed takes into account the size of the components, making it possible to perform parametric analysis on how their area influences the performance of the cycle and to investigate the scale-up of the plant.

A compressible 1D model of the turbo-expander [47] was also developed in EES and added to the absorption cycle model. The model takes into account the behaviour as a real-gas mixture of the working fluid and includes a description of the expansion occurring in the supersonic injector. It is important to highlight that, since the injector of the turbine is a supersonic nozzle, the treated mass flow rate in choking conditions only depends on upstream conditions, and in particular is linearly dependent on the total inlet pressure. As a reminder, for an ideal gas (characterised by an adiabatic index  $\gamma_a$ ) entering an injector of minimum section  $A_{throat}$  with a total inlet pressure and temperature of  $P_{i,tot}$  and  $T_{i,tot}$  respectively, the maximum mass flow rate treated in choking conditions can be written as (SI units):

$$\dot{m}_{max} = \frac{P_{i,tot} A_{throat}}{\sqrt{R T_{i,tot}}} \cdot \sqrt{\gamma_a \cdot \left(\frac{2}{\gamma_a + 1}\right)^{\frac{\gamma_a + 1}{\gamma_a - 1}}} \quad (4)$$

The developed model taking into account real-gas behaviour, mass flow rate maximization is used to calculate the mass flow rate treated by the turbine [48]. Two isentropic efficiencies were considered for the expansion taking place in the nozzle and the recompression from the injector outlet to the rotor inlet. An energy balance allows then calculating the entry speed into the rotor. This is used to find the ideal work  $W_{t,id}$  exchanged by the fluid with the moving blades using Euler's equation [49]:  $W_{t,id} = U \cdot (C_{u,1} - C_{u,2})$ . The turbine's velocity triangle is shown in **Fig. 2**, where  $U$  indicates the rotational speed of the turbine,  $C_{u,1}$  and  $C_{u,2}$  are the tangential component of the absolute flow velocity at the inlet and outlet of the rotor respectively. In the model, the approach was chosen of subtracting loss terms from the theoretical work that can be produced from the rotor inlet kinetic energy. In particular, 4 loss terms within the rotor were considered, their expression taken from literature adjusting coefficients on CFD simulation performed on the turbine [39]:

- passage loss  $\Delta h_{pass}$ , due to fluid dynamic friction in mobile blades and non-optimal incidence angle of the jet incoming to the rotor blades
- friction loss  $\Delta h_{fr}$ , due to the resistance to motion encountered by the vaneless surfaces of the rotor
- leaking loss  $\Delta h_{lk}$ , due to leaking of the working fluid outside the active blade channels not performing work
- partial admission loss  $\Delta h_{pa}$

Full admission turbines generally have higher efficiencies than partial admission turbines, but in circumstances that do not permit full admission such as for very low mass flow rates, partial admission turbines are used. However, when turbines have a high degree of partial admission, related loss can become the major source of loss [50][51].

The isentropic efficiency of the expander is then calculated as follows:

$$\eta_{is,tur} = \frac{W_{t,id} - \Delta h_{pass} - \Delta h_{fr} - \Delta h_{lk} - \Delta h_{pa}}{\Delta h_{is}} \quad (5)$$

where  $\Delta h_{is}$  is the available isentropic enthalpy drop. Results of the turbine model show a mean average error with respect to CFD results lower than 7% [39]. Since partial admission losses depend on the partial admission ratio (i.e. the ratio of active to total blades), when the number of injectors is increased, the efficiency of the turbine increases as well.

The superheater integrated in the pilot plant is electric resistance heater. This choice guarantees a better control of the plant during the experimental campaign but would not be a suitable option for a real machine, particularly for larger plant sizes. Hence, the superheater is also modelled as a plate heat exchanger, but a fixed overall heat transfer coefficient  $K$  of  $300 \text{ W/m}^2\text{K}$  [52] is considered. The calculation of the superheater area, needed for cost estimation, is performed using the LMTD (logarithmic mean temperature difference) method [53]:

$$S_{sh} = \frac{\dot{Q}_{sh}}{K_{sh} \cdot \Delta T_{lm}} \quad (6)$$

where  $\Delta T_{lm}$  represents the mean temperature difference between the HTF and the working fluid. The hot temperature HTF is assumed to first to feed the superheater and then enter the desorber. Hence the superheater HTF mass flow rate is equal to the desorber HTF mass flow rate,  $T_{sh,i}$  is equal to the available hot source temperature and  $T_{d,i} = T_{sh,o}$ .

More details about the absorption chiller and turbine models are available in references [38] and [39].

### 3.2. Exergy analysis

The method of exergy analysis provides insights that may elude a purely first principle analysis, enabling the identification of the irreversibility occurring in a system as well as the evaluation of their magnitude [34].

Exergy is the maximum theoretical useful work obtainable from a system of interest interacting to equilibrium with an idealized system called environment [54] (here  $T_0 = 25^\circ\text{C}$  and  $P_0 = 1.013\text{ bar}$ ). Unlike energy, exergy is not generally conserved and can be destroyed by thermodynamic irreversibility. Considering a steady state control volume, the exergy balance states that the rate at which exergy is transferred into the control volume cannot be smaller than the rate at which exergy is transferred out, the difference being the destroyed exergy  $\dot{E}x_D$ :

$$\sum_j (\dot{E}x_{i,j} + \dot{E}x_{Q,i,j}) = \sum_j (\dot{E}x_{o,j} + \dot{E}x_{Q,o,j}) + \dot{W}_{cv} + \dot{E}x_D \quad (7)$$

$\dot{E}x_{Q,j}$  is the thermal exergy, associated to heat transfer out or into the control volume and defined as:

$$\dot{E}x_{Q,j} = \left(1 - \frac{T_0}{T_j}\right) \cdot \dot{Q}_j \quad (8)$$

$\dot{W}_{cv}$  represents the rate of energy transfer of work other than flow work and  $\dot{E}x_i$  and  $\dot{E}x_o$  are exergy transfer rates at inlet and outlet. In the absence of nuclear, magnetic, electrical and surface tension effects, they can be divided into four components [34]: physical exergy  $Ex^{PH}$ , chemical exergy  $Ex^{CH}$ , kinetic exergy  $Ex^{KN}$  and potential exergy  $Ex^{PT}$ . Kinetic and potential exergy are usually neglected [55] and therefore the total exergy of a stream becomes the sum of physical and chemical exergy [33]:

$$\dot{E}x = \dot{m} \cdot ex = \dot{E}x^{PH} + \dot{E}x^{CH} \quad (9)$$

The physical exergy is associated to the temperature and pressure of a stream of matter and is given by the following expression:

$$\dot{E}x^{PH} = \dot{m} \cdot ex^{PH} = \dot{m} \cdot [(h - h_0) - T_0 \cdot (s - s_0)] \quad (10)$$

Physical exergy does not take into account the exergy component associated to the departure of the chemical composition of a system from that of the environment, which can be evaluated through chemical exergy. The calculation of chemical exergy based on standard (referred to  $T_0 = 25^\circ\text{C}$  and  $P_0 = 1.013\text{ bar}$ ) chemical exergy values of respective species is detailed, among others, by Bejan et al. [34] and Szargut et al. [54]. For the ammonia-water APC cycle considered, the chemical exergy of the flows is calculated using the following relation:

$$\dot{E}x^{CH} = \dot{m} \cdot ex^{CH} = \dot{m} \cdot \left[ \left(\frac{x}{M_{NH_3}}\right) \cdot ex_{NH_3,CH}^0 + \left(\frac{1-x}{M_{H_2O}}\right) \cdot ex_{H_2O,CH}^0 \right] \quad (11)$$

where  $x$  is the ammonia mass fraction, while  $ex_{NH_3,CH}^0$  and  $ex_{H_2O,CH}^0$  are the standard chemical exergy of ammonia and water respectively, and their values are taken from Szargut et al. [54]. In **Eq. (11)**, the mixing effect (i.e.,  $RT_0 \sum_i [x_i \cdot \ln(x_i)]$ ) is neglected given its small magnitude with respect to other terms [56].

As exergy gives information about the quality of energy, the exergetic efficiency provides a true measure of the performance of a system. In order to define this parameter, it is necessary to identify both a product and a fuel of the system studied. The product is the desired useful effect, while the fuel represents the resources spent to generate the product. An exergy rate balance for the system can be then written as:

$$\dot{E}x_F = \dot{E}x_P + \dot{E}x_L + \dot{E}x_D \quad (12)$$

where  $\dot{E}x_F$  is the fuel exergy,  $\dot{E}x_P$  is the product exergy,  $\dot{E}x_L$  is the exergy loss (the exergy associated with the heat rejected to the environment) and  $\dot{E}x_D$  is the exergy destroyed. The exergy efficiency is the ratio between the product and fuel exergy:

$$\eta_{ex} = \frac{\dot{E}x_P}{\dot{E}x_F} \quad (13)$$

The definition of a product and the calculation of an exergy efficiency is not immediate for all components when considering them individually (**Table 4**). For example, this is the case of throttling valves, exchangers crossing  $T_0$  (usually the case of the subcooler in this cycle) or cooling heat exchangers, like the condenser, that serve other components. In addition, a comparison of exergy efficiencies of dissimilar devices is generally not meaningful [34].

**Table 4.** Fuel, product and loss definition for the system.

Component	Fuel	Product	Loss
Absorber	$\dot{E}x_{F,a} = \dot{E}x_{17} + \dot{E}x_6 - \dot{E}x_9$	–	$\dot{E}x_{L,a} = \dot{E}x_{a,o} - \dot{E}x_{a,i}$
Condenser	$\dot{E}x_{F,c} = \dot{E}x_8 - \dot{E}x_9$	–	$\dot{E}x_{L,c} = \dot{E}x_{c,o} - \dot{E}x_{c,i}$
Desorber	$\dot{E}x_{F,d} = \dot{E}x_{d,i} - \dot{E}x_{d,o}$	$\dot{E}x_{P,d} = \dot{E}x_7 + \dot{E}x_4 - \dot{E}x_3$	–
Electric generator	$\dot{E}x_{F,ele} = \dot{W}_t$	$\dot{E}x_{P,ele} = \dot{W}_{t,ele}$	–
Evaporator	$\dot{E}x_{F,e} = \dot{E}x_{11} - \dot{E}x_{12}$	$\dot{E}x_{P,e} = \dot{E}x_{e,o} - \dot{E}x_{e,i}$	–
Mix cooling and power	$\dot{E}x_{F,mix} = \dot{E}x_{17} - \dot{E}x_{16} - \dot{E}x_{13}$	–	–
Pump	$\dot{E}x_{F,p} = \dot{W}_p$	$\dot{E}x_{P,p} = \dot{E}x_2 - \dot{E}x_1$	–
Refrigerant expansion valve	$\dot{E}x_{F,refvalv} = \dot{E}x_{10} - \dot{E}x_{11}$	–	–
Solution expansion valve	$\dot{E}x_{F,solvalv} = \dot{E}x_5 - \dot{E}x_6$	–	–
Solution heat exchanger	$\dot{E}x_{F,shx} = \dot{E}x_4 - \dot{E}x_5$	$\dot{E}x_{P,shx} = \dot{E}x_3 - \dot{E}x_2$	–
Subcooler	$\dot{E}x_{F,sub} = \dot{E}x_9 - \dot{E}x_{10}$	$\dot{E}x_{P,sub} = \dot{E}x_{13} - \dot{E}x_{12}$	–
Superheater	$\dot{E}x_{F,sh} = \dot{E}x_{sh,i} - \dot{E}x_{sh,o}$	$\dot{E}x_{P,sh} = \dot{E}x_{15} - \dot{E}x_{14}$	–
Turbine	$\dot{E}x_{F,t} = \dot{E}x_{15} - \dot{E}x_{16}$	$\dot{E}x_{P,t} = \dot{W}_t$	–
Overall system	$\dot{E}x_F = \dot{E}x_{d,i} - \dot{E}x_{d,o} + \dot{E}x_{sh,i} - \dot{E}x_{sh,o}$	$\dot{E}x_P = \dot{W}_{ele,net} + \dot{E}x_{e,i} - \dot{E}x_{e,o}$	$\dot{E}x_L = \dot{E}x_{c,o} - \dot{E}x_{c,i} + \dot{E}x_{a,o} - \dot{E}x_{a,i}$

However, applying **Eq.(12)** and using the definitions of **Table 4**, it is possible to calculate the values of the rates of exergy destroyed ( $\dot{E}x_{D,k}$ ) and exergy loss ( $\dot{E}x_{L,k}$ ) in each component  $k$  and in the overall system ( $\dot{E}x_D$  and  $\dot{E}x_L$ ). It is then interesting to calculate the ratio of exergy destruction and exergy loss ratios, expressed as follows:

$$Y_{D,k} = \frac{\dot{E}x_{D,k}}{\dot{E}x_F} \quad (14)$$

$$Y_{D,k}^* = \frac{\dot{E}x_{D,k}}{\dot{E}x_D} \quad (15)$$

$$Y_{L,k} = \frac{\dot{E}x_{L,k}}{\dot{E}x_F} \quad (16)$$

While the rates of  $\dot{E}x_{D,k}$  and  $\dot{E}x_{L,k}$  give a thermodynamic measure of the system inefficiencies,  $Y_{D,k}$ ,  $Y_{D,k}^*$  and  $Y_{L,k}$  are useful to compare different components of the same system.

### 3.3. Performance evaluation parameters

In addition to the cooling and electrical power outputs, both first and second law based performance criteria are used here to evaluate the combined cycle performance. Since the desorbed vapour is divided between the cooling and the electrical power production line, the split ratio is used to measure the fraction of vapour passing through the cooling production line:

$$r_s = \frac{\dot{m}_{11}}{\dot{m}_7} \quad (17)$$

It is important to highlight that  $r_s$  is not a control parameter of the system, but rather an output variable. Indeed, the area of the system's heat exchangers fixes the mass flow rate of desorbed vapour for a specific operating point. On the other hand, the mass flow rate treated by the turbine is also fixed in a given operating point, and depending only on conditions upstream of the turbine and on its geometry [39]. The vapour mass flow rate passing through the cooling part of the circuit is hence the difference between the total desorbed vapour mass flow rate and the mass flow rate treated by the turbine.

The system first-law efficiency  $\eta_I$  (sometimes referred to as energy utilization factor [52]) is defined as the ratio of useful outputs (cooling and net electrical power) to the total driving thermal energy inputs [57]:

$$\eta_I = \frac{\dot{W}_{ele,net} + \dot{Q}_e}{\dot{Q}_d + \dot{Q}_{sh}} \quad (18)$$

In **Eq. (18)** the net electrical power generated by the cycle is calculated as:  $\dot{W}_{ele,net} = \eta_{gen} \cdot \eta_{mech} \cdot \dot{W}_t - \dot{W}_p = \dot{W}_{t,ele} - \dot{W}_p$  [58], where  $\eta_{gen}$  is the electric generator efficiency and  $\eta_{mech}$  is the mechanical coupling efficiency, fixed to 96% and 98% respectively [59].  $\dot{Q}_e$ ,  $\dot{Q}_d$  and  $\dot{Q}_{sh}$  represents respectively the powers exchanged by the evaporator, desorber and superheater.

However, as observed in [60], **Eq. (18)** overestimates the efficiency of the cycle by giving the same value to the cooling and electrical power outputs of the system. To avoid misleading results, the authors suggested the use of a modified first law efficiency, replacing cooling power output  $\dot{Q}_e$  with the exergy associated with the refrigeration output  $\dot{E}x_{P,e} = \dot{E}x_{e,o} - \dot{E}x_{e,i}$ :

$$\eta_{I,eff} = \frac{\dot{W}_{ele,net} + \dot{E}x_{P,e}}{\dot{Q}_d + \dot{Q}_{sh}} \quad (19)$$

Also the modified expression of **Eq. (19)** fails to account for the quality of the thermal input, thus not reflecting all the losses due to irreversibility in a cycle. Hence, to evaluate the true value of useful outputs of the cycle, exergy efficiency must be used [61]. Following the definition in **Eq. (13)**, the exergy efficiency of the system considered can be written following definitions in **Table 4** as [62]:

$$\eta_{ex} = \frac{\dot{W}_{ele,net} + (\dot{E}x_{e,o} - \dot{E}x_{e,i})}{(\dot{E}x_{d,i} - \dot{E}x_{d,o}) + (\dot{E}x_{sh,i} - \dot{E}x_{sh,o})} = \frac{\dot{W}_{ele,net} + \dot{E}x_{P,e}}{\dot{E}x_{F,d} + \dot{E}x_{F,sh}} \quad (20)$$

## 4. Exergoeconomic analysis

### 4.1. Cost balance equations

Exergoeconomics is the branch of engineering that combines exergy analysis and economic principles [34]. It is based on the idea that exergy is the only true thermodynamic measure to value the interactions that a system experiences with its surroundings, and therefore the only meaningful way to assign a monetary cost to them. An exergoeconomic (or thermoeconomic) analysis is particularly useful when dealing with complex systems with more than one useful product, like the combined system under investigation. Indeed, a thermoeconomic analysis allows calculating separately the cost of each product generated by the system, understanding the cost formation process and optimising specific variables in a single component or in the overall system. This approach, referred to as exergy costing, consists in associating a cost rate  $\dot{C}$  to each exergy stream entering the system:

$$\dot{C}_i = c_i \cdot \dot{E}x_i; \quad \dot{C}_o = c_o \cdot \dot{E}x_o; \quad \dot{C}_w = c_w \cdot \dot{W}; \quad \dot{C}_Q = c_Q \cdot \dot{E}x_Q \quad (21)$$

In **Eq. (21)**,  $c_{in}$ ,  $c_{out}$ ,  $c_w$  and  $c_Q$  denote the average cost per unit of exergy in dollars per joule (\$/J). Exergy costing involves applying a cost balance, usually formulated for each component  $k$  of the system, stating that the total cost of the streams exiting are equal to the expenditure to obtain them:

$$\sum_i \dot{C}_{i,k} + \dot{C}_{Q,k} + \dot{Z}_k = \sum_o \dot{C}_{o,k} + \dot{C}_{w,k} \quad (22)$$

Here, the right term represents the total cost rate of the energy streams exiting the system, while the left term of the equation represents the cost rate necessary to generate them.  $\dot{Z}_k$  (\$/s) is the total cost rate associated with capital investment (CI) and operating and maintenance costs (O&M) needed to own and operate component  $k$ :

$$\dot{Z}_k = \dot{Z}_{CI,k} + \dot{Z}_{OM,k} \quad (23)$$

Since costs vary from year to year levelized cost are considered when evaluating cost of a thermal system. Consequently, costs in **Eq. (23)** are to be intended as levelized costs and in particular  $\dot{Z}_{CI,k}$  represents the total capital investment, while  $\dot{Z}_{OM,k}$  represent operating and maintenance expenditures. The hourly levelized capital investment can be calculated for component  $k$  as:

$$\dot{Z}_{CI,k} = \left( \frac{CRF}{\tau} \right) \cdot Z_k \quad (24)$$

where  $\tau$  is the number of yearly operating hours,  $Z_k$  is the capital investment cost of the component and CRF is the capital recovery factor calculated as:

$$CRF = \frac{i_r \cdot (1 + i_r)^n}{(1 + i_r)^n - 1} \quad (25)$$

In **Eq. (25)**,  $i_r$  indicates the interest rate and the  $n$  the number of useful years. The annual levelized O&M costs for component  $k$  is given by [34]:

$$\dot{Z}_{OM,k} = \frac{\gamma_k \cdot Z_k}{\tau} + \omega_k \cdot \dot{E}_{Xp,k} + \dot{R}_k \quad (26)$$

where  $\gamma_k$  and  $\omega_k$  are associated with fixed and variable O&M costs respectively.  $\dot{R}_k$  comprises all other operation and maintenance costs independent of investment costs and product exergy. Since  $\omega_k \cdot \dot{E}_{Xp,k}$  and  $\dot{R}_k$  are significantly smaller than  $\frac{\gamma_k \cdot Z_k}{\tau}$ , they are most often neglected [34]. Therefore the annual levelized cost for component  $k$  can finally be written as:

$$\dot{Z}_k = \left( \frac{CRF}{\tau} \right) \cdot Z_k + \left( \frac{\gamma_k}{\tau} \right) \cdot Z_k \quad (27)$$

In this study the investment lifetime  $n$  is assumed to be 20 years [12], the interest rate  $i_r$  10 % [52], the number of operating hours is 8000 [12][63] and the maintenance factor  $\gamma_k$  taken is 0.06 [58][64] for all components. Capital cost functions used for each component, expressed in US dollars, are shown in **Table 5**. These data are brought to a reference year (2021) using the chemical engineering plant cost index (CEPCI) [65]:

$$Z_{year2} = Z_{year1} \cdot \left( \frac{CEPCI_{year2}}{CEPCI_{year1}} \right) \quad (28)$$

Cost correlation for plate heat exchangers is based on French cost in 2021 and obtained using data from 8 different heat exchangers. Indeed, vendor's price quote or data from previously bought similar equipment are the best way to estimate cost [66]. Heat exchangers cost correlations are often formulated as [67]:

$$Z = k_1 + k_2 \cdot S^m \quad (29)$$

in which the exponent  $m$  to which the exchanger area  $S$  is raised is usually smaller than one. The exponent used here, 0.67, is in agreement with the six-tenths rule [68], stating that when costs of a component are known, but its area ( $S_b$ ) differs from that of the to be estimated component ( $S_a$ ), costs can be roughly estimated using the correlation:

$$\frac{Z_a}{Z_b} = \left( \frac{S_a}{S_b} \right)^n \quad (30)$$

The exponent  $n$  differs per type of equipment, but  $s$  is often comprised between 0.5-0.7 for thermal systems [34]. In the base case of heat exchanger area of 1 m<sup>2</sup>, using the correlation in **Table 5** results in slightly higher cost than the widely used [69] linear correlation proposed by Quoilin [70] for plate heat exchangers, also reported in the table as a term of comparison.

**Table 5.** Cost functions for the economic modelling of the system ( $\dot{W}_t, \dot{W}_{t,ele}, \dot{W}_{pump}$  in  $kW$  and  $S$  in  $m^2$ )

Component	Capital investment cost function	Reference	Year	CEPCI
Ammonia turbine (TUR)	$4405 \cdot \dot{W}_t^{0.7}$	[52][58]	2005	468
Generator and electrical auxiliaries	$10^7 \cdot \left( \frac{\dot{W}_{t,ele}}{1.6 \cdot 10^5} \right)^{0.7}$	[58]	1998	389
Heat exchangers	$130 + 564 \cdot S^{0.67}$	-	2021	700
Heat exchangers (alternative correlation)	$130 + 310 \cdot S$	[71]	2010	551
Pump	$1120 \cdot \dot{W}_p^{0.8}$	[52][58]	2005	468

As done in the case of the fuel and product exergy (**Table 4**), also in the case of exergy costing all the components of the system are considered as individual units, as also assumed for example in [58]. **Table 6** lists all cost rate balance and auxiliary equations for each system component. Since only the costs of the streams entering the system are known (left term in **Eq. (22)**), when the product definition for a component involves  $m$  exiting streams,  $m - 1$  auxiliary equations must be formulated.

**Table 6.** Exergetic cost rate balance and auxiliary equations for the system.

Component	Cost rate balance equation	Auxiliary equations
Absorber	$\dot{C}_{a,i} + \dot{C}_{17} + \dot{C}_6 + \dot{Z}_{abs} = \dot{C}_{a,o} + \dot{C}_1$	$c_{a,i} = c_{a,o} = 0$
Condenser	$\dot{C}_{c,i} + \dot{C}_8 + \dot{Z}_{cond} = \dot{C}_{a,o} + \dot{C}_9$	$c_{c,i} = c_{c,o} = 0$
Desorber	$\dot{C}_{d,i} + \dot{C}_3 + \dot{Z}_{des} = \dot{C}_{d,o} + \dot{C}_7 + \dot{C}_4$	$\frac{\dot{C}_7 - \dot{C}_3}{\dot{Ex}_7 - \dot{Ex}_3} = \frac{\dot{C}_4 - \dot{C}_3}{\dot{Ex}_e - \dot{Ex}_3}; \quad c_{d,i} = c_{d,o} = c_{fuel}$
Electric generator	$\dot{C}_{ele} = \dot{Z}_{gen} + \dot{C}_t$	-
Evaporator	$\dot{C}_{e,i} + \dot{C}_{11} + \dot{Z}_{evap} = \dot{C}_{e,o} + \dot{C}_{12}$	$c_{11} = c_{12}$
Mix cooling and power lines	$\dot{C}_{13} + \dot{C}_{16} = \dot{C}_{17}$	-
Pump	$\dot{C}_1 + \dot{C}_{pump} + \dot{Z}_{pump} = \dot{C}_2$	$c_{pump} = c_t$
Refrigerant expansion valve	$\dot{C}_{10} + \dot{Z}_{refvalv} = \dot{C}_{11}$	-
Solution expansion valve	$\dot{C}_5 + \dot{Z}_{solvalv} = \dot{C}_6$	-
Solution heat exchanger	$\dot{C}_4 + \dot{C}_2 + \dot{Z}_{shx} = \dot{C}_3 + \dot{C}_4$	$c_4 = c_5$
Subcooler	$\dot{C}_9 + \dot{C}_{12} + \dot{Z}_{sub} = \dot{C}_{10} + \dot{C}_{13}$	$c_{12} = c_{13}$
Superheater	$\dot{C}_{sh,i} + \dot{C}_{14} + \dot{Z}_{sh} = \dot{C}_{sh,o} + \dot{C}_{15}$	$c_{sh,i} = c_{sh,o} = c_{fuel}$
Turbine	$\dot{C}_{15} + \dot{Z}_t = \dot{C}_t + \dot{C}_{16}$	$c_{15} = c_{16}$

The cooling water used in the condenser and in the absorber is considered as a free resource [58] and hence its cost per unit of exergy is neglected [72] ( $c_{a,i} = 0$  and  $c_{c,i} = 0$ ). In the same way, the cost of the exergy of the fluid at the evaporator inlet is assumed to be null [58]. The auxiliary equation most often encountered in literature [58][33][12] in the case of a condenser is to assume that the cost per unit of exergy of the working mixture remains constant between condenser inlet and outlet ( $c_8 = c_9$ ). However, in this way the cost rate of the component,  $\dot{Z}_{cond}$ , is charged to the outlet water used to cool down the condenser. Additionally, since the working mixture undergoes an exergy reduction in the condenser, but the specific exergy cost is assumed to be constant, the cost of the exergy stream at the condenser outlet,  $\dot{C}_9 = c_9 \cdot \dot{Ex}_9$ , is smaller than the cost at inlet  $\dot{C}_8$  (as evident from Table 7 in reference [58]). This cost difference also being charged to the cooling water, the overall result is that of a reduction of the cost of the products, which would be smaller than the sum of the total CI and O&M costs of components ( $\sum \dot{Z}_k$ ) and fuel costs.

Indeed, all the costs associated with owning and operating a component should be charged to the product of that component [34]. In the case of the condenser in this study, the useful effect of the component is not the heating of the cooling water, but the condensation of the working fluid. Consequently, the auxiliary equation used for the condenser in this study is  $c_{c,i} = c_{c,o} = 0$ . Considering that  $\dot{Ex}_{co} - \dot{Ex}_{ci}$  is an exergy loss, this is coherent with what suggested by Bejan et al. [34] with respect to costing of exergy losses. The authors [34] state that the approach to follow when dealing with exergy losses finally discharged to the environment should be to impose  $\dot{C}_{L,k} = 0$ , so that the product bears the full burden of the costs associated with component  $k$ . This is also coherent with the approach proposed by the same authors [34] for cooling heat exchangers.

The same approach was followed in the case of the absorber, where the auxiliary equation  $c_{a,i} = c_{a,o} = 0$  was used.

## 4.2. Exergoeconomic parameters

Exergoeconomic parameters play an important role in the evaluation and in the optimization of thermal systems. The most used ones are the average unit cost of fuel  $c_{F,k}$ , the average unit cost of products  $c_{P,k}$ , the cost rate of exergy destruction  $\dot{C}_{D,k}$ , the cost rate of exergy loss  $\dot{C}_{L,k}$ , and the exergoeconomic factor  $f_k$  [34], defined as:

$$c_{F,k} = \frac{\dot{C}_{F,k}}{\dot{E}x_{F,k}} \quad (31)$$

$$c_{P,k} = \frac{\dot{C}_{P,k}}{\dot{E}x_{P,k}} \quad (32)$$

$$\dot{C}_{D,k} = c_{F,k} \cdot \dot{E}x_{D,k} \quad (33)$$

$$\dot{C}_{L,k} = c_{F,k} \cdot \dot{E}x_{L,k} \quad (34)$$

$$f_k = \frac{\dot{Z}_k}{\dot{Z}_k + \dot{C}_{D,k} + \dot{C}_{L,k}} \quad (35)$$

The cost of exergy destruction and loss calculated with **Eq. (33)** and **Eq. (34)** can be interpreted as the cost rate of the additional fluid that must be supplied to component  $k$  to cover the rate of exergy destruction and loss. Another definition for the two quantities is possible by using the specific cost of the product  $c_{P,k}$  instead of  $c_{F,k}$  in **Eq. (33)** and **Eq. (34)**. This formulation is equivalent to considering  $\dot{C}_{D,k}$  and  $\dot{C}_{L,k}$  as the monetary loss associated with the loss of product [34]. In reality, neither expression is strictly correct, with the actual cost being in the middle between the two resulting values. Using **Eq. (33)** and **Eq. (34)** is however a more conservative approach with respect to capital investment, and therefore these expressions are more commonly used [58] [31].

The exergoeconomic factor  $f_k$  can be very useful in the identification of design changes that could improve the cost-effectiveness of a thermal system. The exergoeconomic factor measures the relative importance of two types of cost sources: exergy related costs (exergy destroyed and loss) and non-exergy related costs (CI and O&M costs). When  $f_k$  is very high for a component  $k$ , costs savings for the entire system could be achieved by reducing the investment cost of the component, at the price of lowering its exergetic performance. On the other hand, low values of  $f_k$  indicate the possibility of increasing the exergoeconomic performance of the system by increasing the capital investment for the component to improve its exergy efficiency.

After solving the system equations listed in **Table 6**, the specific cost of electricity ( $c_{ele} = \dot{C}_{ele}/\dot{W}_{t,ele}$ ) and the specific cost of cooling ( $c_{cooling} = \dot{C}_{e,o}/(\dot{E}x_{e,o} - \dot{E}x_{e,i})$ ) can be calculated using **Eq. (32)**. The overall unit cost of product for the system is obtained through the following equation [31]:

$$c_{prod} = c_{cooling} + c_{ele} \quad (36)$$

The unit cost of produced exergy (*UCOPE*) is another useful parameter to analyse the system from an economic point of view. For systems with more than one product *UCOPE* can be defined as [31]:

$$UCOPE = \frac{\sum \dot{Z}_k + \sum (c_{F,k} \cdot \dot{E}x_{F,k})}{\sum \dot{E}x_P} \quad (37)$$

For the system considered, in light of the discussion in **Section 4.1** and of equations in **Table 6**, the *UCOPE* can be written for this system as:

$$UCOPE = \frac{\dot{C}_{e,o} + \dot{C}_{ele} + c_F \cdot (\dot{E}x_{F,d} + \dot{E}x_{F,sh})}{\dot{E}x_{P,e} + \dot{W}_{t,ele}} = \frac{c_{cooling} \cdot (\dot{E}x_{e,o} - \dot{E}x_{e,i}) + c_{ele} \cdot \dot{W}_{t,ele}}{(\dot{E}x_{e,o} - \dot{E}x_{e,i}) + \dot{W}_{t,ele}} \quad (38)$$

showing that the *UCOPE* is a weighted average on the useful exergy of each product of their relative specific cost. Finally, one last important parameter for the evaluation of the exergoeconomic performance of the system is the sum of the capital investment cost rate and of the total exergy destruction for each component ( $\sum \dot{Z}_k + \sum \dot{C}_{D,k}$ ).

## 5. Results and discussion

The system thermodynamic and exergoeconomic performance is analysed in **Section 5.1** for the pilot plant design operating conditions and for a base case operating point characterised by a hot source temperature of 100 °C, intermediate temperature source of 25 °C and evaporator inlet temperature of 10 °C, representing a space cooling

application. For the base case conditions, the performance achievable by increasing of 25 times the size of the plant (so that a full admission turbine can be used) is evaluated.

A parametric study on the temperature of the sources is then performed in **Section 5.2** to assess the impact of the hot and cold source temperatures, all other conditions being fixed. The impact of heat exchangers area is also evaluated. Finally, in **Section 5.3** an optimization is performed for the scaled-up plant in order to find the optimal exchangers area minimizing the unit cost of produced exergy (*UCOPE*) of the system.

### 5.1. Pilot plant results and scale-up evaluation

Simulations of the cycle were conducted using the model presented in **Section** Erreur ! Source du renvoi introuvable.. Two operating points are evaluated (**Table 7**), the design point of the pilot plant and a base case representative of a typical refrigeration application, for which also the effect of scaling-up the plant is studied. The temperature of the hot source HTF considered is 100 °C, while the temperature of the cold source HTF considered are 18 °C and 10 °C respectively (corresponding to an outlet cooled HTF temperature  $T_{e,o}$  of 15.4°C and 7.3 °C respectively). The hot temperature HTF is used first to supply thermal power to the superheater and then to the desorber (hence  $T_{sh,o} = T_{d,i}$ ).

**Table 7.** Input parameters and predicted performance of the pilot plant at nominal and base case operating points.

Parameters	Nominal point	Base case	Scale-up x25
<b>Input parameters</b>			
Hot source temperature, $T_{sh,i}$ [°C]	100	100	100
Intermediate source temperature, $T_{a,i}$ and $T_{c,i}$ [°C]	25	25	25
Cold source temperature, $T_{e,i}$ [°C]	18	10	10
Rich solution mass flow rate, $\dot{m}_1$ [kg/h]	100	100	2 500
<b>Thermal power exchangers</b>			
Absorber, $\dot{Q}_a$ [kW]	12.76	11.73	297
Condenser, $\dot{Q}_c$ [kW]	4.45	3.75	101
Desorber, $\dot{Q}_d$ [kW]	13.10	12.09	310
Evaporator - Cooling power, $\dot{Q}_e$ [kW]	3.93	3.31	90
Superheater, $\dot{Q}_{sh}$ [kW]	0.31	0.28	7
<b>Turbine</b>			
Turbine isentropic efficiency, $\eta_{is,tur}$ [%]	40.6	44.1	73.2
Rotational speed turbine, $\omega$ [rpm]	39 200	49 500	80 000
Mechanical power turbine, $\dot{W}_t$ [kW]	0.16	0.24	10
Electrical power turbine, $\dot{W}_{t,ele}$ [kW]	0.15	0.22	9.5
Net electrical power cycle, $\dot{W}_{ele,net}$ [kW]	0.13	0.20	8.9
<b>Overall performance indicators</b>			
Cooled water temperature, $T_{e,o}$ [°C]	14.9	7.3	7.2
Desorbed vapour mass flow rate, $\dot{m}_8$ [kg/h]	28.78	26.21	679
Split Ratio, $\tau_s$ [-]	0.43	0.39	0.41
First law efficiency, $\eta_f$ [%]	30.27	28.41	31.17
Effective first law efficiency, $\eta_{I,eff}$ [%]	1.81	3.18	4.44
Exergy efficiency, $\eta_{ex}$ [%]	9.37	16.45	22.96
<b>Exergoeconomic performance for <math>c_F = 0</math> \$/GJ</b>			
Exergoeconomic factor, $f$ [-]	1	1	1
Unit cost of produced cooling, $c_{cooling}$ [\$/GJ]	175 (0.63 \$/kWh)	96 (0.35 \$/kWh)	14.8 (0.05\$/kWh)
Unit cost of produced electricity, $c_{ele}$ [\$/GJ]	1 681 (6.05 \$/kWh)	1 073 (3.86 \$/kWh)	45 (0.16 \$/kWh)
Unit cost of products, $c_{prod}$ [\$/GJ]	1 856 (6.68 \$/kWh)	1 169 (4.21 \$/kWh)	59.8 (0.21 \$/kWh)
Unit cost of produced exergy, <i>UCOPE</i> [\$/GJ]	1 012 (3.64 \$/kWh)	626 (2.25 \$/kWh)	34.2 (0.12 \$/kWh)
<b>Exergoeconomic performance for <math>c_F = 15</math> \$/GJ</b>			
Exergoeconomic factor, $f$ [-]	0.87	0.88	0.39
Unit cost of produced cooling, $c_{cooling}$ [\$/GJ]	292 (1.05 \$/kWh)	160 (0.58 \$/kWh)	75 (0.27 \$/kWh)
Unit cost of produced electricity, $c_{ele}$ [\$/GJ]	1 879 (6.76 \$/kWh)	1 190 (4.28 \$/kWh)	113 (0.41 \$/kWh)
Unit cost of products, $c_{prod}$ [\$/GJ]	2 171 (7.81 \$/kWh)	1 350 (4.86 \$/kWh)	188 (0.68 \$/kWh)
Unit cost of produced exergy, <i>UCOPE</i> [\$/GJ]	1 174 (4.22 \$/kWh)	718 (2.58 \$/kWh)	99 (0.35 \$/kWh)

The scale-up of the heat exchangers is performed so as not to affect their effectiveness with respect to operation in the pilot plant (i.e. leaving dimensionless parameters shown in **Table 3** constant). In this study, this is done simply by increasing the number of plates of the heat exchangers. Although this is not the way heat exchangers would be scaled in reality, the assumption is that the same exchangers effectiveness could be achieved with well designed heat exchangers also at larger sizes. Since heat exchangers area would increase less than linearly with exchanged power in real life applications, linearly increasing the number of plates as done here gives an upper cost estimation.

When scaling-up the desorber the hypothesis is made that the ratio between adiabatic and heated plates surface is equal to the one of the pilot plant (35 %) to guarantee the same vapour purity.

Since the design point of the turbine (inlet pressure of 16 bar and outlet pressure of 4 bar) is quite different from the actual cycle operating conditions (**Table A1-A3**), the flow at the injector outlet is over-expanded and shock phenomena take place, affecting the performance of the turbine. Performance analysis using the turbine model shows that a converging-only injector is optimal for the conditions under investigation. Hence, this configuration is retained for the study. For each case considered in **Table 7** and in **Fig. 3**, the optimal rotational speed maximizing the turbine efficiency is found. Additionally, it is assumed that the reduced number of injectors linked to a partial admission turbine does not entail a significant cost reduction. Thus, the cost of the turbine is considered equal to the cost of a full-admission turbine (mechanical power estimated from simulations in **Table 7** of around 10 kW) also in the case of partial admission configurations. It is worth mentioning that the cost calculated for  $\dot{W}_t = 10$  kW using the correlation of **Table 5** brought to the reference year of 2021, is higher than the actual cost of turbine integrated in the pilot plant, which was however designed for a higher pressure ratio.

The specific cost of the thermal input,  $c_{fuel}$ , is an important parameter determining the cost of the products. Different values of this parameter can be found in literature: [58] and [73] assumed it to be waste heat with negligible cost, [25][74][75] considered it to be vapour with cost of 15.24 \$/GJ while [31] considered a cost of 17.85 \$/GJ. Two different scenarios are analysed in the present study: the use of waste heat with negligible cost and the use of a fuel with a cost of 15 \$/GJ, to assess how the exergoeconomic performance of the plant is affected by the cost of the fuel.

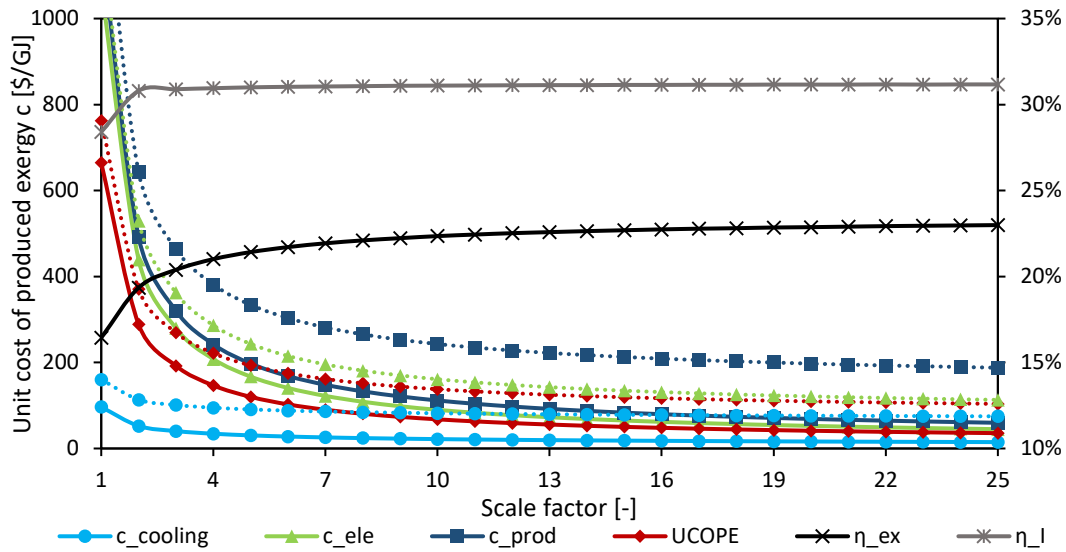


**Fig. 3.** Change of energy efficiency, exergy efficiency and UCOPE (bold lines for the case of  $c_F = 0$  \$/GJ, dotted lines for the case of  $c_F = 15$  \$/GJ) increasing the plant size with respect to the pilot plant size.

At the nominal point, the system absorbs 13.10 kW from the hot source (considering both  $\dot{Q}_d$  and  $\dot{Q}_{sh}$ ), producing 3.93 kW of cooling at 14.9 °C and 130 W of net electrical output. The high pressure of the cycle determines the mass flow rate treated by the turbine, corresponding in the design point to approximately 57% of the desorbed vapour ( $\tau_s=0.43$ ). The first law efficiency of the cycle is 30.27 %, while the exergy efficiency 9.37 %.

For the base case considered, the lower cooling output temperature increases the exergy efficiency of the system (**Section 5.2**). This is due to the fact that the cooling power output remains almost constant but its exergetic value is higher as a consequence of the lower temperature. Additionally, the low pressure of the cycle being determined by the evaporating temperature ( $T_{11}$ ), the pressure drop available to the turbine increases, increasing the power

production of the expander. As a consequence the unit cost of produced exergy decreases, with an UCOPE passing from 1012 \$/GJ to 654 \$/GJ in the case of  $c_F = 0$  and from 1174 \$/GJ to 762 \$/GJ in the case of  $c_F = 15$  \$/GJ.

**Fig. 3** shows for the base case operating point the effect of increasing the plant size, measured by the scale factor (i.e. the relative area of heat exchangers, working fluid and HTF mass flow rate values with respect to the pilot plant area). It can be seen how the specific cost of products decreases significantly when increasing the plant size. This is due to the fact that components cost increases less than linearly with their size, and to the fact that the turbine cost, the major cost item (**Table 8**), remains constant. Moreover, reducing the partial admission ratio improves the isentropic efficiency of the turbine  $\eta_{is,tur}$ , reaching 73.2 % in the case of a full admission turbine. This leads to an increase in the exergy efficiency of the system, passing from 16.45 % to 22.96 % which is not reflected however in an equal increase in the first law efficiency. As a result, the cost  $c_{cooling}$  is 14.8 (75) \$/GJ,  $c_{ele}$  is 45 (113) \$/GJ,  $c_{prod}$  is 59.8 (188) \$/GJ and the UCOPE 34.2 (99) \$/GJ for a plant 25 times bigger than the pilot plant for  $c_F = 0$  ( $c_F = 15$  \$/GJ respectively). **Appendix B** shows the outputs of the exergoeconomic analysis when using alternative heat exchangers cost correlations proposed by [71]. Predicted cost of products in this case are very similar at the pilot plant size and slightly higher for the scaled-up plant.

**Table 8.** Exergy and exergoeconomic indicators for the system components and overall system for the case of the scaled up plant (scale factor 25) and  $c_F = 15$ \$/GJ.

Component	$\dot{E}x_{Dk}$ [kW]	$\dot{E}x_{Lk}$ [kW]	$Y_{D,k}$ [-]	$Y_{D,k}^*$ [-]	$Y_{L,k}$ [-]	$\dot{Z}_{,k}$ [\$/h]	$\dot{C}_{D,k}$ [\$/h]	$\dot{C}_{L,k}$ [\$/h]	$f_k$ [-]
Absorber	18.18	-	0.295	0.425	0.073	0.10	0.98	0.23	0.10
Condenser	1.80	0.49	0.029	0.042	0.009	0.13	0.10	0.03	0.52
Desorber	11.45	4.17	0.186	0.268	-	0.12	0.62	-	0.16
Electric generator	0.60	-	0.010	0.014	-	0.42	0.03	-	0.93
Evaporator	1.32	-	0.021	0.031	-	0.09	0.07	-	0.57
Mix cooling and power	0.23	-	0.004	0.005	-	0.00	0.01	-	0.00
Pump	0.12	-	0.002	0.003	-	0.02	0.01	-	0.94
Refrigerant expansion valve	0.09	-	0.001	0.002	-	0.00	0.00	-	0.00
Solution expansion valve	0.32	-	0.005	0.007	-	0.00	0.02	-	0.00
Solution heat exchanger	4.92	-	0.080	0.115	-	0.05	0.27	-	0.16
Subcooler	0.06	-	0.001	0.001	-	0.04	0.00	-	0.93
Superheater	0.26	-	0.004	0.006	-	0.02	0.01	-	0.59
Turbine	3.42	-	0.056	0.080	-	0.73	0.18	-	0.80
Overall system	42.76	4.66	0.695	1.000	0.082	1.75	2.31	0.25	0.40

The values of exergy destroyed and lost in each component, and the ratios of exergy destroyed relative to the net fuel exergy supplied ( $Y_{D,k}$ ) and relative to the total exergy destruction in the system ( $Y_{D,k}^*$ ) are shown in **Table 8**. The absorber and the desorber are the primary contributors total exergy destruction ( $Y_{D,k}^*$  of 42.5% and 26.8% respectively), followed by the solution heat exchanger and turbine. **Table 8** also shows exergoeconomic analysis results in the case of  $c_F = 15$  \$/GJ (for  $c_F = 0$  \$/GJ,  $\dot{C}_{D,k}$  and  $\dot{C}_{L,k}$  would always be equal to 0). The turbine and the electric generator present the highest values of  $\dot{Z}_{,k}$  (0.73 \$/h and 0.42 \$/h respectively), but have a relatively low cost of exergy destruction compared to the absorber, desorber and solution heat exchanger. The low values of the exergoeconomic factor for these components indicates that cost savings could possibly be achieved by increasing their size and efficiency (and hence their cost). In contrast, the pump, turbine and electric generator have high exergoeconomic factors indicating that capital cost rates could be decreased at the expense of a reduced component efficiency. The overall exergoeconomic factor for the system is 0.4 and 53.7% of total costs for the system (2.31\$/h) come from exergy destruction.

Stream thermodynamic properties and cost data corresponding to the three cases shown in **Table 7** are presented in **Appendix A**.

## 5.2. Parametric analysis

The influence of the temperature of the hot and cold sources on the thermodynamic and exergoeconomic performance of the cycle is evaluated in **Fig. 4**. Reducing the evaporator temperature increases the exergy efficiency of the cycle, up to a maximum depending on the hot and medium source temperatures. The maximum

reachable value of the exergy efficiency changes little in the temperature range studied, but the hot source temperature maximising the exergy efficiency increases when reducing the cold source temperature. On the other hand, the first principle efficiency of the cycle is substantially reduced at lower evaporator temperature because the cooling power production decreases. This is due to the fact that the mass flow rate of circulating refrigerant vapour decreases at lower evaporator temperatures (determining the low pressure of the cycle) mainly because the absorption process becomes less efficient at lower pressure. Since the mass flow rate treated by the turbine remains constant, the mass flow rate passing through the cooling line of the cycle is reduced, as shown by the split ratio tending to zero for temperatures below 4 °C in the case of a hot source temperature of 100 °C (**Fig. 4(a)**).

Also the exergoeconomic performance of the cycle is strongly affected by the temperature of the sources. In particular, the higher the temperature of the hot source the more convenient it is to produce cooling at lower temperature. However, also in this case, there exists a temperature minimising the *UCOPE*. In the case of ambient temperature of 25 °C and hot source temperature of 100 °C, this temperature is slightly below 10 °C, corresponding to the base case under investigation.

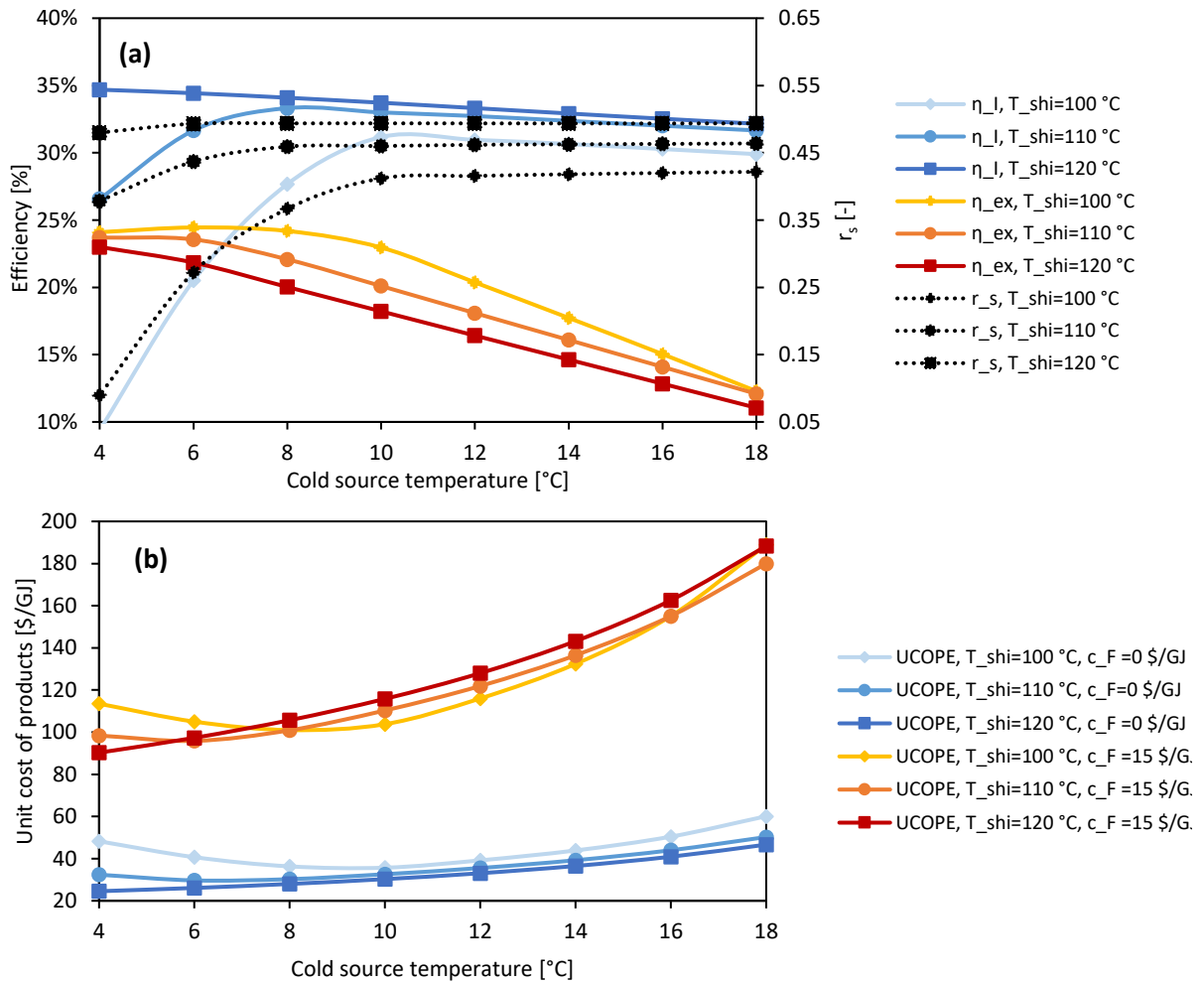


**Fig. 4.** Impact of the temperature of the cold and hot source on the thermodynamic (a) and exergoeconomic performance of the cycle (b) for an ambient temperature of 25 °C.

Subsequently, the influence of the heat exchangers area on the performance of the cycle was analysed. **Fig. 5** presents results concerning the size of the absorber, the component with the highest value of the sum of  $\dot{Z}_k + \dot{C}_{D,k}$  (**Table 8**), and hence the first to address in an optimization procedure. Increasing the size of the absorber initially reduces the *UCOPE*, because the thermodynamic efficiency of the cycle increase. However, further increasing the absorber area increases capital costs more than the cost savings linked to reduced exergy destruction. An optimization of components size minimizing the *UCOPE* is presented in the next section.

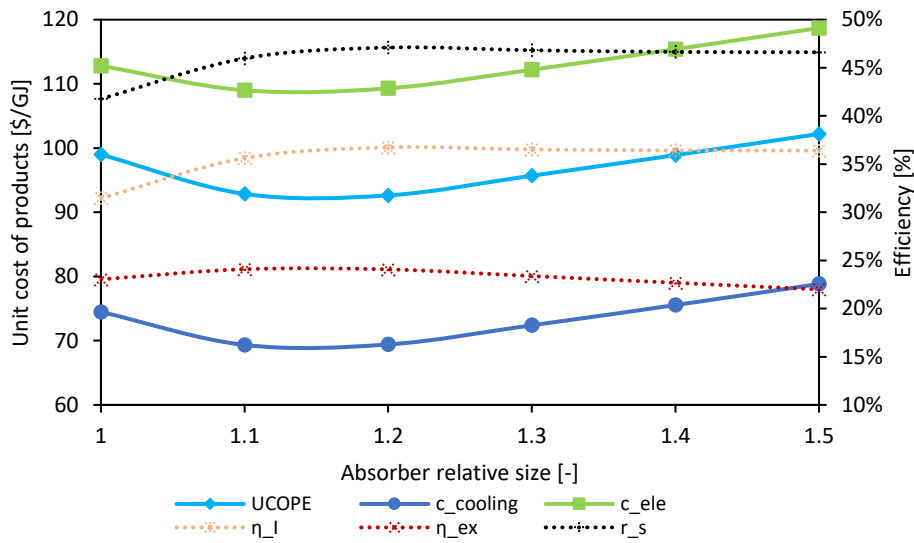


**Fig. 5.** Impact of the absorber area with respect to the scaled up plant in the base case operating point for  $c_F = 15\$/GJ$ .

### 5.3. Optimization

Exergoeconomic optimization aims at maximizing thermal and exergy efficiencies and minimizing the cost of products simultaneously. Objective functions can vary widely, depending on the desired decision variable, and optimization criteria can be based on maximizing first principle or exergy efficiency or at minimizing the cost per unity of exergy of the products (i.e.  $UCOPE$ ,  $c_{prod}$ ,  $c_{ele}$ ,  $c_{cooling}$ ). In this work, the  $UCOPE$  is considered as the most significant variable representing the exergoeconomic performance of the cycle. An optimisation is carried out aiming at minimizing its value in the base case working point (hot source temperature  $100^\circ$ , intermediate source temperature  $25^\circ C$  and cold source temperature  $10^\circ C$ ), by varying the area of the system heat exchangers. More specifically, the size of the turbine and the solution mass flow rate are kept constant, while heat exchangers area is varied looking for the optimal trade-off between their cost and performance in the system under investigation.

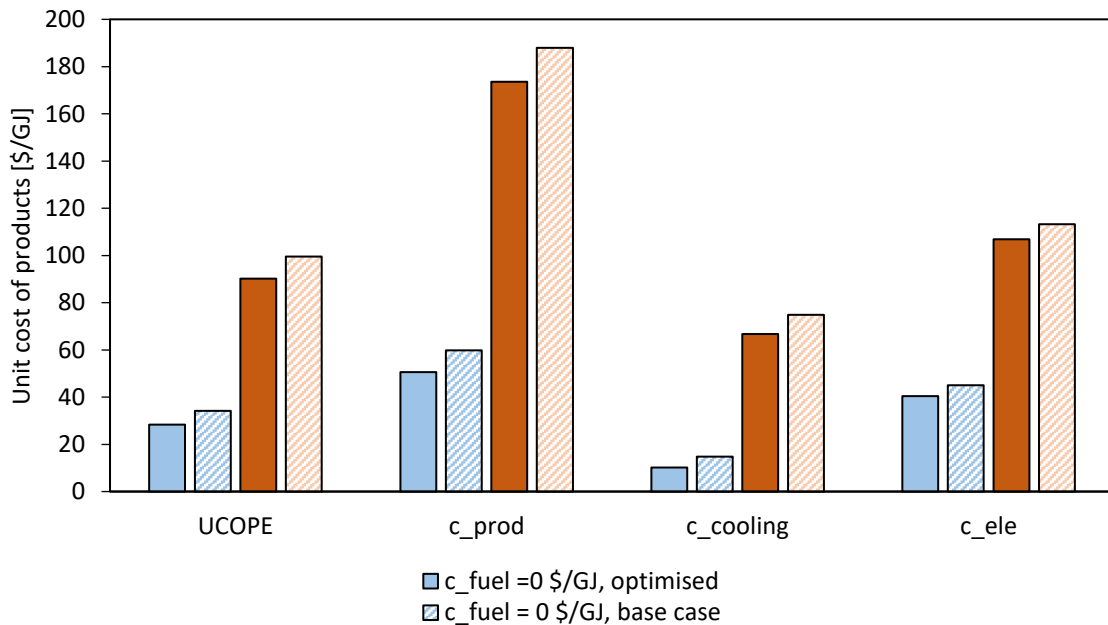


**Fig. 6.** Heat exchangers size optimization results.

Several optimization methods are available in the EES software [76]. The EES internal genetic algorithm, used in several studies [25][75][77], has the advantage of being the most robust and not being affected by the guess values of the independent variables as is the case for direct search and variable metric methods. However, the genetic method is the slowest of the available methods and Zare et al. [25] concluded that by assigning appropriate guess values for the parameters, the genetic algorithm and direct search methods yield the same optimization results. Since reliable guess values for the optimal area of components are available from parametric studies on exchangers area (like the one presented for the absorber in **Section 5.2**), the direct search method was used in this study. This method, also commonly used in literature [56], is based on an iterative search intended to find an optimum by directly comparing function values at a sequence of trial points without involving derivatives.

**Table 9.** Exergy and exergoeconomic indicators for the optimised configurations.

<b>Thermodynamic and exergoeconomic performance parameters</b>	<b><math>c_F = 0</math> \$/GJ</b>	<b><math>c_F = 15</math> \$/GJ</b>
Unit cost of produced exergy, $UCOPE$ [\$GJ]	28.31 (0.101 \$/kWh)	90.24 (0.324 \$/kWh)
Unit cost of products, $c_{prod}$ [\$GJ]	50.58 (0.182 \$/kWh)	173.5 (0.624 \$/kWh)
Unit cost of produced electricity, $c_{ele}$ [\$GJ]	40.45 (0.146 \$/kWh)	106.8 (0.384 \$/kWh)
cost of produced cooling, $c_{cooling}$ [\$GJ]	10.14 (0.036 \$/kWh)	66.7 (0.240 \$/kWh)
Exergy efficiency, $\eta_{ex}$ [%]	23.8	24.2
First law efficiency, $\eta_l$ [%]	35.7	36.5
Split Ratio, $r_s$ [-]	0.46	0.47
Evaporator - Cooling power, $\dot{Q}_e$ [kW]	116.1	119.6
Net electrical power cycle, $\dot{W}_{ele,net}$ [kW]	9.8	9.5
<b>Heat exchangers relative area with respect to base case</b>		
Relative area absorber [-]	1.14	1.14
Relative area condenser [-]	0.48	0.79
Relative area desorber [-]	1.2	1.01
Relative area evaporator [-]	0.49	0.72
Relative area solution heat exchanger [-]	1.09	1.04
Relative area subcooler [-]	0.51	0.86
Relative area superheater [-]	1.25	1.43
Total Capital cost, $\sum \dot{Z}_k$ [\$h]	1.71	1.75

**Fig. 6** outlines the results of the optimization process both in the case of  $c_F$  equal to 0 and 15 \$/GJ. In the first case the  $UCOPE$  is reduced of 17.2 % with respect to the base case in **Table 7**, down to reaching 28 \$/GJ, while in the second case the  $UCOPE$  is reduced of 8.8% up to reaching 90.8 \$/GJ. The relatively small  $UCOPE$  reduction indicates that the pilot plant is well designed. **Table 9** also presents the relative area of heat exchangers resulting from the optimization, with respect to the linear scale up of the plant presented in **Table 7**. It can be noticed that overall the total capital cost do not change much compared to results in **Table 8** ( $\sum \dot{Z}_k = 1.75$  \$/h), with a small reduction in the case of  $c_F = 0$  \$/GJ, where, since the cost of the fuel is neglected, higher exergetic losses are acceptable. This is due to two main reasons. The first is that the major cost item, the cost of the turbine (accounting together with the electrical generator for a capital cost of 1.15 \$/h in the base case) is kept constant. The second reason is that the resulting optimal area increases for some exchangers while decrease for others. The optimal area of the absorber, for example, is found to be around 14% bigger than in the base case. This is not surprising since the absorber of the pilot plant has been designed for a nominal cold source temperature of 18 °C, and hence benefiting from a higher working pressure.

On the other hand the optimal area of heat exchangers of the cooling production line is found to be significantly smaller than in the base case. Also this is not surprising, since in the pilot plant had been designed to treat all the desorbed mass flow rate, but the addition of the turbine deviates a considerable part of it (around 60%) to the power production line. Finally, for the optimal configuration the split ratio increases with respect to the base case, reaching 0.47.

## 6. Conclusions

The scale-up of an ammonia-water combined refrigeration and electrical power production is investigated in this paper from a thermodynamic and exergoeconomic point of view. The study is based on an experimental ammonia-water absorption chiller prototype developed ad CEA INES to which an impulse axial turbine was integrated.

Previously developed models of the absorption chiller and of the turbine, allowing evaluation of their scale-up, are presented briefly.

Fixing the hot source temperature to 100 °C, the performance of the prototype is analysed in the design working point and in a base case characterised respectively by a cold source temperature of 18 °C and 10 °C respectively. The supersonic turbine appears to impose strict limits on the cycle in terms of treated mass flow rate, not allowing the possibility of regulating the vapour split ratio between the cooling and electricity production line. On the other hand, this is imposed by the relative size of turbine and heat exchangers.

The small size of the pilot plant (thermal power input of 12-13 kW) proves to be very penalizing for the *UCOPE*, in particular because of the very high cost of the partial-admission turbine. For this reason the effect of increasing the plant size of 25 times (up to reach full admission conditions for the turbine) is evaluated for the base case working point. In this case, the cycle produces around 90 kW of cooling at around 7 °C and about 9 kW of electricity reaching and exergy efficiency of 23 %.

A parametric study performed on the temperature of the sources highlights their strong influence on the performance of the cycle and shows that for given conditions of the hot and intermediate source temperature, there is a cooling production temperature maximizing exergy efficiency or minimizing the *UCOPE*.

Finally, fixing the size of the turbine and the solution mass flow rate, an optimisation of the area of heat exchangers is performed to minimise the *UCOPE* for two different cost of the fuel: the use of waste heat having negligible cost and the use of a thermal input with a cost of 15 \$/GJ.

When the fuel cost is neglected the optimisation process leads to an *UCOPE* of 28.31 \$/GJ, while when the cost of fuel is 15 \$/GJ the optimal *UCOPE* is 90.24 \$/GJ. The higher cost per unity of exergy of electricity production compared to cooling would seem to suggest favouring the production of cooling.

## Declaration of Competing Interest

The authors declare that they have no known competing financial interests or personal relationships that could have appeared to influence the work reported in this paper.

## Acknowledgements

The authors would like to express their gratitude to the French Alternative Energies and Atomic Energy Commission and the Carnot Energies of the Future Institute. S. Braccio was supported by the CEA NUMERICS program, which has received funding from the European Union Horizon 2020 research and innovation program under the Marie Skłodowska-Curie grant agreement No 800945. The authors would like to thank the University Savoie Mont Blanc and CEA Grenoble for funding research stay at KU Leuven of S. Braccio.

## Appendix A

**Table A1.** State properties and costs of the system in the nominal point of the pilot plant.

Stream	$T_i$ [°C]	$P_i$ [bar]	$h_i$ [kJ/kg]	$s_i$ [kJ/kgK]	$\dot{m}_i$ [kg/h]	$x_i$ [-]	$\dot{E}x_i^{PH}$ [kW]	$\dot{E}x_i^{CH}$ [kW]	$c_{fuel} = 0$ \$/GJ		$c_{fuel} = 15$ \$/GJ	
									$c_i$ [\$/GJ]	$\dot{C}_i$ [\$/h]	$c_i$ [\$/GJ]	$\dot{C}_i$ [\$/h]
1	28.60	6.27	-109.8	0.270	100	0.535	0.9	295.3	98.57	105.1	179.80	191.7
2	28.66	10.54	-109.1	0.270	100	0.535	0.9	295.3	98.67	105.2	179.90	191.8
3	62.52	10.54	81.6	0.862	100	0.535	1.3	295.3	98.74	105.4	180.00	192.2
4	94.50	10.54	204.9	1.191	71	0.351	0.6	138.4	98.00	49.1	178.80	89.5
5	33.92	10.54	-62.8	0.396	71	0.351	0.0	138.4	98.03	48.9	178.80	89.1
6	34.01	6.27	-62.8	0.397	71	0.351	0.0	138.4	98.03	48.9	178.80	89.1
7	67.84	10.54	1415.0	4.707	29	0.989	2.7	156.9	98.18	56.4	179.10	102.9
8	67.84	10.54	1415.0	4.708	12	0.989	1.1	67.5	98.18	24.3	179.10	44.3
9	26.95	10.54	119.3	0.459	12	0.989	1.0	67.5	98.40	24.3	179.40	44.3
10	16.41	10.54	69.1	0.288	12	0.989	1.0	67.5	98.43	24.3	179.50	44.3
11	10.86	6.27	69.1	0.291	12	0.989	1.0	67.5	98.43	24.3	179.50	44.3
12	15.86	6.27	1213.0	4.293	12	0.989	0.9	67.5	98.43	24.2	179.50	44.2
13	22.80	6.27	1263.0	4.464	12	0.989	0.9	67.5	98.43	24.2	179.50	44.2
14	67.84	10.54	1415.0	4.707	16	0.989	1.5	89.4	98.18	32.1	179.10	58.6
15	95.00	10.54	1485.0	4.904	16	0.989	1.6	89.4	98.14	32.1	179.00	58.6
16	74.58	6.27	1451.0	5.051	16	0.989	1.2	89.4	98.14	32.0	179.00	58.4
17	48.49	6.27	1370.0	4.808	29	0.989	2.1	156.9	98.28	56.3	179.20	102.6

**Table A2.** State properties and costs of the system in the base case point of the pilot plant.

Stream	$T_i$ [°C]	$P_i$ [bar]	$h_i$ [kJ/kg]	$s_i$ [kJ/kgK]	$\dot{m}_i$ [kg/h]	$x_i$ [-]	$\dot{E}x_i^{PH}$ [kW]	$\dot{E}x_i^{CH}$ [kW]	$c_{fuel} = 0$ \$/GJ		$c_{fuel} = 15$ \$/GJ	
									$c_i$ [\$/GJ]	$\dot{C}_i$ [\$/h]	$c_i$ [\$/GJ]	$\dot{C}_i$ [\$/h]
1	32.34	4.71	-94.5	0.326	100	0.514	0.7	284.1	61.31	62.9	112.10	114.9
2	32.43	10.35	-93.6	0.326	100	0.514	0.7	284.1	61.39	63.0	112.20	115.0
3	65.15	10.35	91.0	0.894	100	0.514	1.2	284.1	61.44	63.1	112.30	115.3
4	94.76	10.35	207.3	1.195	74	0.346	0.7	141.5	61.04	31.2	111.70	57.1
5	38.15	10.35	-42.9	0.457	74	0.346	0.0	141.5	61.06	31.1	111.70	56.9
6	38.26	4.71	-42.9	0.459	74	0.346	0.0	141.5	61.07	31.1	111.70	56.9
7	70.20	10.35	1424.0	4.743	26	0.987	2.4	142.6	61.05	31.9	111.70	58.3
8	70.20	10.35	1424.0	4.743	10	0.987	0.9	56.0	61.05	12.5	111.70	22.9
9	26.44	10.35	115.2	0.451	10	0.987	0.9	56.0	61.23	12.5	111.90	22.9
10	8.79	10.35	31.8	0.164	10	0.987	0.9	56.0	61.27	12.5	112.00	22.9
11	2.86	4.71	31.8	0.168	10	0.987	0.9	56.0	61.28	12.5	112.00	22.9
12	7.86	4.71	1190.0	4.336	10	0.987	0.6	56.0	61.28	12.5	112.00	22.8
13	21.56	4.71	1274.0	4.626	10	0.987	0.6	56.0	61.28	12.5	112.00	22.8
14	70.20	10.35	1424.0	4.743	16	0.987	1.5	86.6	61.05	19.4	111.70	35.4
15	95.00	10.35	1488.0	4.921	16	0.987	1.5	86.6	61.04	19.4	111.60	35.4
16	63.28	4.71	1433.0	5.133	16	0.987	1.0	86.6	61.04	19.3	111.60	35.2
17	45.02	4.71	1371.0	4.941	26	0.987	1.6	142.6	61.14	31.7	111.80	58.0

**Table A3.** State properties and costs of the streams in the base case for the scaled-up plant (scale factor 25).

Stream	$T_i$ [°C]	$P_i$ [bar]	$h_i$ [kJ/kg]	$s_i$ [kJ/kgK]	$\dot{m}_i$ [kg/h]	$x_i$ [-]	$\dot{E}x_i^{PH}$ [kW]	$\dot{E}x_i^{CH}$ [kW]	$c_{fuel} = 0$ \$/GJ		$c_{fuel} = 15$ \$/GJ	
									$c_i$ [\$/GJ]	$\dot{C}_i$ [\$/h]	$c_i$ [\$/GJ]	$\dot{C}_i$ [\$/h]
1	31.28	4.71	-99.0	0.310	2500	0.519	19.10	7169	7.94	205.6	56.01	1449
2	31.37	10.39	-98.1	0.310	2500	0.519	19.59	7169	7.95	205.7	56.02	1450
3	64.68	10.39	92.3	0.897	2500	0.519	30.35	7169	7.96	206.2	56.06	1453
4	95.32	10.39	210.4	1.203	1821	0.344	16.66	3472	7.90	99.2	55.79	700.7
5	36.09	10.39	-51.1	0.430	1821	0.344	0.99	3472	7.90	98.8	55.79	697.5
6	36.20	4.71	-51.1	0.432	1821	0.344	0.67	3472	7.90	98.8	55.80	697.5
7	69.91	10.39	1423	4.738	679	0.988	62.36	3697	7.91	107.0	55.83	755.5
8	69.91	10.39	1423	4.738	280	0.988	25.69	1523	7.91	44.1	55.83	311.3
9	26.55	10.39	116.0	0.453	280	0.988	23.40	1523	7.95	44.2	55.93	311.4
10	8.79	10.39	32.0	0.164	280	0.988	23.57	1523	7.95	44.3	55.94	311.5
11	2.86	4.71	32.0	0.168	280	0.988	23.48	1523	7.95	44.3	55.95	311.5
12	7.86	4.71	1192	4.343	280	0.988	16.91	1523	7.95	44.1	55.95	310.2
13	21.93	4.71	1276	4.635	280	0.988	16.68	1523	7.95	44.1	55.95	310.1
14	69.91	10.39	1423	4.738	399	0.988	36.67	2174	7.91	62.9	55.83	444.3
15	95.00	10.39	1487	4.918	399	0.988	37.84	2174	7.91	63.0	55.81	444.4
16	49.94	4.71	1396	5.021	399	0.988	24.34	2174	7.91	62.6	55.81	441.6
17	39.65	4.71	1347	4.866	679	0.988	40.78	3697	7.92	106.7	55.87	751.8

## Appendix B. Alternative heat exchangers cost correlation

**Table B1.** Exergoeconomic parameters results for the cases in **Table 7** using heat exchangers cost correlations from [70]

Parameters	Nominal point	Base case	Scale-up x25
<b>Exergoeconomic performance for <math>c_{fuel} = 0</math> \$/GJ</b>			
Exergoeconomic factor, $f$ [-]	1	1	1
Unit cost of produced cooling, $c_{cooling}$ [\$GJ]	165 (0.60 \$/kWh)	93 (0.33 \$/kWh)	26 (0.09 \$/kWh)
Unit cost of produced electricity, $c_{ele}$ [\$GJ]	1394 (5.02 \$/kWh)	1070 (3.85 \$/kWh)	52 (0.19 \$/kW)
Unit cost of products, $c_p$ [\$GJ]	1559 (5.62\$/kWh)	1163 (4.18 \$/kWh)	78 (0.28 \$/kWh)
Unit cost of produced exergy, $UCOPE$ [\$GJ]	1036 (3.73 \$/kWh)	660 (2.38 \$/kWh)	43 (0.15 \$/kWh)
<b>Exergoeconomic performance for <math>c_{fuel} = 15</math> \$/GJ</b>			
Exergoeconomic factor, $f$ [-]	0.87	0.88	0.41
Unit cost of produced cooling, $c_{cooling}$ [\$GJ]	275 (0.99 \$/kWh)	156 (0.56 \$/kWh)	86 (0.31 \$/kWh)
Unit cost of produced electricity, $c_{ele}$ [\$GJ]	1563 (5.62 \$/kWh)	1186 (4.27 \$/kWh)	121 (0.43 \$/kW)
Unit cost of products, $c_p$ [\$GJ]	1838 (6.61 \$/kWh)	1342 (4.83 \$/kWh)	207 (0.74 \$/kWh)
Unit cost of produced exergy, $UCOPE$ [\$GJ]	1197 (4.31 \$/kWh)	758 (2.73 \$/kWh)	108 (0.40 \$/kWh)

## 7. References

- [1] F. Birol, "The Future of Cooling-Opportunities for energy efficient air conditioning- Opportunities for energy efficient air conditioning," *OECD/IEA 2018*, 2018.
- [2] R. Best and W. Rivera, "A review of thermal cooling systems," *Appl. Therm. Eng.*, vol. 75, pp. 1162–1175, 2015, doi: 10.1016/j.applthermaleng.2014.08.018.
- [3] S. Ajib and W. Günther, "Solar thermally driven cooling systems: Some investigation results and perspectives," *Energy Convers. Manag.*, vol. 65, pp. 663–669, 2013, doi: 10.1016/j.enconman.2011.09.022.
- [4] K. E. Herold, R. Radermacher, and S. A. Klein, *Absorption Chillers and Heat Pumps*, Second. CRC Press, 2016. doi: 10.1201/b19625.
- [5] D. B. Boman, A. W. Raymond, and S. Garimella, *Absorption Heat Pumps: Fundamentals and Applications*. Springer International Publishing, 2021. doi: <https://doi.org/10.1007/978-3-030-72180-0>.
- [6] I. P. Koronaki, E. Rogdakis, and T. Kakatsiou, "Experimental assessment and thermodynamic analysis of a solar desiccant cooling system," *Int. J. Sustain. Energy*, vol. 32, no. 2, pp. 121–136, Apr. 2013, doi: 10.1080/14786451.2012.666551.
- [7] T. Katejanekarn, S. Chirattananon, and S. Kumar, "An experimental study of a solar-regenerated liquid desiccant ventilation pre-conditioning system," *Sol. Energy*, vol. 83, no. 6, pp. 920–933, 2009, doi: <https://doi.org/10.1016/j.solener.2008.12.006>.
- [8] G. Besagni, R. Mereu, and F. Inzoli, "Ejector refrigeration: A comprehensive review," *Renewable and Sustainable Energy Reviews*. 2016. doi: 10.1016/j.rser.2015.08.059.
- [9] R. Ventas, C. Vereda, A. Lecuona, and M. Venegas, "Experimental study of a thermochemical compressor for an absorption/compression hybrid cycle," *Appl. Energy*, vol. 97, pp. 297–304, 2012, doi: <https://doi.org/10.1016/j.apenergy.2011.11.052>.
- [10] A. I. Kalina, "Combined-Cycle System With Novel Bottoming Cycle," *J. Eng. Gas Turbines Power*, vol. 106, no. 4, pp. 737–742, Oct. 1984, doi: 10.1115/1.3239632.
- [11] E. Macchi, "Theoretical basis of the Organic Rankine Cycle," in *Organic Rankine Cycle (ORC) Power Systems: Technologies and Applications*, Woodhead Publishing, 2016. doi: 10.1016/B978-0-08-100510-1.00001-6.
- [12] M. Akbari Kordlar and S. M. S. Mahmoudi, "Exergeconomic analysis and optimization of a novel cogeneration system producing power and refrigeration," *Energy Convers. Manag.*, vol. 134, pp. 208–220, 2017, doi: 10.1016/j.enconman.2016.12.007.
- [13] D. S. Ayou, J. C. Bruno, R. Saravanan, and A. Coronas, "An overview of combined absorption power and cooling cycles," *Renewable and Sustainable Energy Reviews*, vol. 21. Elsevier, pp. 728–748, 2013. doi: 10.1016/j.rser.2012.12.068.
- [14] X. Chen, R. Z. Wang, and S. Du, "An improved cycle for large temperature lifts application in water-ammonia absorption system," *Energy*, vol. 118, pp. 1361–1369, 2017, doi: <https://doi.org/10.1016/j.energy.2016.11.014>.
- [15] P. Srihirin, S. Aphornratana, and S. Chungpaibulpatana, "A review of absorption refrigeration technologies," *Renewable and Sustainable Energy Reviews*. 2000. doi: 10.1016/S1364-0321(01)00003-X.
- [16] Q. Blondel, N. Tauveron, N. Caney, and N. Voeltzel, "Experimental study and optimization of the Organic Rankine Cycle with pure Novec<sup>TM</sup>649 and zeotropic mixture Novec<sup>TM</sup>649/HFE7000 as working fluid," *Appl. Sci.*, 2019, doi: 10.3390/app9091865.
- [17] V. Zare, "A comparative thermodynamic analysis of two tri-generation systems utilizing low-grade geothermal energy," *Energy Convers. Manag.*, vol. 118, pp. 264–274, 2016, doi: <https://doi.org/10.1016/j.enconman.2016.04.011>.
- [18] V. Novotny and M. Kolovratnik, "Absorption power cycles for low-temperature heat sources using aqueous salt solutions as working fluids," *Int. J. Energy Res.*, vol. 41, no. 7, pp. 952–975, 2017, doi: 10.1002/er.3671.
- [19] A. Khaliq, "Energetic and exergetic performance investigation of a solar based integrated system for cogeneration of power and cooling," *Appl. Therm. Eng.*, vol. 112, pp. 1305–1316, 2017, doi: 10.1016/j.applthermaleng.2016.10.127.
- [20] F. Xu, D. Yogi Goswami, and S. S. Bhagwat, "A combined power/cooling cycle," *Energy*, 2000, doi: 10.1016/S0360-5442(99)00071-7.
- [21] G. P. Kumar, R. Saravanan, and A. Coronas, "Experimental studies on combined cooling and power system driven by low-grade heat sources," *Energy*, vol. 128, pp. 801–812, 2017, doi: 10.1016/j.energy.2017.04.066.
- [22] J. Wang, Y. Dai, T. Zhang, and S. Ma, "Parametric analysis for a new combined power and ejector-absorption refrigeration cycle," *Energy*, vol. 34, no. 10, pp. 1587–1593, 2009, doi:

- 10.1016/j.energy.2009.07.004.
- [23] D. Y. Goswami and F. Xu, "Analysis of a New Thermodynamic Cycle for Combined Power and Cooling Using Low and Mid Temperature Solar Collectors," *J. Sol. Energy Eng.*, vol. 121, pp. 91–97, 1999, doi: <https://doi.org/10.1115/1.2888152>.
- [24] A. A. Hasan, D. Y. Goswami, and S. Vijayaraghavan, "First and second law analysis of a new power and refrigeration thermodynamic cycle using a solar heat source," *Sol. Energy*, vol. 73, no. 5, pp. 385–393, 2002, doi: 10.1016/S0038-092X(02)00113-5.
- [25] V. Zare, S. M. S. Mahmoudi, M. Yari, and M. Amidpour, "Thermoeconomic analysis and optimization of an ammonia-water power/cooling cogeneration cycle," *Energy*, vol. 47, no. 1, pp. 271–283, 2012, doi: 10.1016/j.energy.2012.09.002.
- [26] N. Zhang and N. Lior, "Development of a novel combined absorption cycle for power generation and refrigeration1," *J. Energy Resour. Technol. Trans. ASME*, vol. 129, no. 3, pp. 254–265, 2007, doi: 10.1115/1.2751506.
- [27] L. Sun, W. Han, X. Jing, D. Zheng, and H. Jin, "A power and cooling cogeneration system using mid/low-temperature heat source," *Appl. Energy*, vol. 112, pp. 886–897, 2013, doi: 10.1016/j.apenergy.2013.03.049.
- [28] L. C. Mendoza, D. S. Ayou, J. Navarro-Esbrí, J. C. Bruno, and A. Coronas, "Small capacity absorption systems for cooling and power with a scroll expander and ammonia based working fluids," *Appl. Therm. Eng.*, vol. 72, no. 2, pp. 258–265, 2014, doi: 10.1016/j.applthermaleng.2014.06.019.
- [29] J. López-Villada, D. S. Ayou, J. C. Bruno, and A. Coronas, "Modelling, simulation and analysis of solar absorption power-cooling systems," *Int. J. Refrig.*, vol. 39, pp. 125–136, 2014, doi: 10.1016/j.ijrefrig.2013.11.004.
- [30] S. M. S. Mahmoudi and M. Akbari Kordlar, "A new flexible geothermal based cogeneration system producing power and refrigeration," *Renew. Energy*, vol. 123, pp. 499–512, 2018, doi: 10.1016/j.renene.2018.02.060.
- [31] N. Shokati, F. Ranjbar, and M. Yari, "A comprehensive exergoeconomic analysis of absorption power and cooling cogeneration cycles based on Kalina, part 1: Simulation," *Energy Convers. Manag.*, vol. 158, no. November 2017, pp. 437–459, 2018, doi: 10.1016/j.enconman.2017.12.086.
- [32] Z. Seyfour, M. Ameri, and M. A. Mehrabian, "Exergo-economic analysis of a low-temperature geothermal-fed combined cooling and power system," *Appl. Therm. Eng.*, vol. 145, no. May, pp. 528–540, 2018, doi: 10.1016/j.applthermaleng.2018.09.072.
- [33] R. D. Misra, P. K. Sahoo, and A. Gupta, "Thermoeconomic evaluation and optimization of an aqua-ammonia vapour-absorption refrigeration system," *Int. J. Refrig.*, vol. 29, no. 1, pp. 47–59, 2006, doi: 10.1016/j.ijrefrig.2005.05.015.
- [34] A. Bejan, G. Tsatsaronis, and M. J. Moran, *Thermal design and optimization*. Wiley, 1995.
- [35] H. Ghaebi, T. Parikhani, and H. Rostamzadeh, "Energy, exergy and thermoeconomic analysis of a novel combined cooling and power system using low-temperature heat source and LNG cold energy recovery," *Energy Convers. Manag.*, vol. 150, pp. 678–692, 2017, doi: <https://doi.org/10.1016/j.enconman.2017.08.052>.
- [36] W. Huang, J. Wang, J. Xia, P. Zhao, and Y. Dai, "Performance analysis and optimization of a combined cooling and power system using low boiling point working fluid driven by engine waste heat," *Energy Convers. Manag.*, vol. 180, pp. 962–976, 2019, doi: <https://doi.org/10.1016/j.enconman.2018.11.041>.
- [37] F. Boudéhenn, H. Demasles, J. Wytenbach, X. Jobard, D. Chèze, and P. Papillon, "Development of a 5 kW cooling capacity ammonia-water absorption chiller for solar cooling applications," *Energy Procedia*, vol. 30, pp. 35–43, 2012, doi: 10.1016/j.egypro.2012.11.006.
- [38] S. Braccio *et al.*, "Simulation of an ammonia-water absorption cycle using exchanger effectiveness.," *Appl. Therm. Eng.*, vol. 213, p. 1, 2022, doi: <https://doi.org/10.1016/j.applthermaleng.2022.118712>.
- [39] S. Braccio, A. Di Nardo, G. Calchetti, H. T. Phan, N. Le Pierrès, and N. Tauveron, "Performance evaluation of a micro partial admission impulse axial turbine in a combined ammonia-water cooling and electricity absorption cycle," 2022.
- [40] S. Braccio, H. T. Phan, N. Tauveron, and N. Le Pierrès, "Study of the integration of a supersonic impulse turbine in a NH<sub>3</sub>/H<sub>2</sub>O absorption heat pump for combined cooling and power production from a low temperature heat source," *E3S Web Conf.*, vol. 312, p. 08018, 2021, doi: 10.1051/e3sconf/202131208018.
- [41] M. Wirtz, B. Stutz, H. T. Phan, and F. Boudehenn, "Combined generator for an NH<sub>3</sub>–H<sub>2</sub>O absorption chiller," *Int. J. Heat Mass Transf.*, vol. 196, p. 123311, 2022, doi: <https://doi.org/10.1016/j.ijheatmasstransfer.2022.123311>.
- [42] M. A. Staedter and S. Garimella, "Direct-coupled desorption for small capacity ammonia-water absorption systems," *Int. J. Heat Mass Transf.*, vol. 127, pp. 196–205, 2018, doi: <https://doi.org/10.1016/j.ijheatmasstransfer.2018.06.118>.

- [43] S. A. Ibrahim, O.M., Klein, “Thermodynamic properties of ammonia-water mixtures.,” in *ASHRAE Trans.: Symposia*, 21, 2, 1495 (1993).
- [44] F. Incropera, *Fundamentals of Heat and Mass Transfer*. Hoboken, NJ, USA: John Wiley & Sons, 2006.
- [45] D. Triché, S. Bonnot, M. Perier-Muzet, F. Boudéhenn, H. Demasles, and N. Caney, “Experimental and numerical study of a falling film absorber in an ammonia-water absorption chiller,” *Int. J. Heat Mass Transf.*, vol. 111, pp. 374–385, 2017, doi: 10.1016/j.ijheatmasstransfer.2017.04.008.
- [46] D. Triche, “Numerical and experimental study of coupled mass and heat transfers in the absorber of an ammonia-water absorption chiller. PhD thesis.,” Université Grenoble Alpes, 2016. [Online]. Available: <https://tel.archives-ouvertes.fr/tel-01696252>
- [47] S. Braccio, H. T. Phan, N. Tauveron, and N. Le Pierrès, “Study of a cold and electric cogeneration machine using a low temperature heat source.,” *SFT 2021*, 2021, doi: <https://doi.org/10.25855/SFT2021-036>.
- [48] S. Braccio, N. Guillou, N. Le Pierrès, N. Tauveron, and H. Trieu Phan, “Mass-flowrate-maximization thermodynamic model and simulation of supersonic real-gas ejectors used in refrigeration systems,” *Therm. Sci. Eng. Prog.*, p. 101615, 2022, doi: <https://doi.org/10.1016/j.tsep.2022.101615>.
- [49] S. Dixon and C. Hall, *Fluid Mechanics and Thermodynamics of Turbomachinery*, Seventh Ed. Butterworth-Heinemann, 2014. doi: <https://doi.org/10.1016/C2011-0-05059-7>.
- [50] S. Y. Cho, C. H. Cho, and C. Kim, “Performance prediction on a partially admitted small axial-type turbine,” *JSME Int. Journal, Ser. B Fluids Therm. Eng.*, vol. 49, no. 4, pp. 1290–1297, 2007, doi: 10.1299/jsmeb.49.1290.
- [51] M. Li, J. Wang, L. Gao, X. Niu, and Y. Dai, “Performance evaluation of a turbine used in a regenerative Organic Rankine Cycle,” in *Proceedings of the ASME Turbo Expo*, 2012, vol. 6, pp. 425–432. doi: 10.1115/GT2012-68441.
- [52] V. Zare, S. M. S. Mahmoudi, and M. Yari, “An exergoeconomic investigation of waste heat recovery from the Gas Turbine-Modular Helium Reactor (GT-MHR) employing an ammonia-water power/cooling cycle,” *Energy*, vol. 61, pp. 397–409, 2013. doi: 10.1016/j.energy.2013.09.038.
- [53] B. H. Gebreslassie, G. Guillén-Gosálbez, L. Jiménez, and D. Boer, “Design of environmentally conscious absorption cooling systems via multi-objective optimization and life cycle assessment,” *Appl. Energy*, vol. 86, no. 9, pp. 1712–1722, 2009, doi: <https://doi.org/10.1016/j.apenergy.2008.11.019>.
- [54] J. Szargut, “Exergy method: technical and ecological applications,” *Int. Ser. Dev. heat Transf.*, vol. 18, p. 164, 2005.
- [55] A. Vidal, R. Best, R. Rivero, and J. Cervantes, “Analysis of a combined power and refrigeration cycle by the exergy method,” *Energy*, vol. 31, no. 15, pp. 3401–3414, 2006, doi: 10.1016/j.energy.2006.03.001.
- [56] V. Zare, S. M. S. Mahmoudi, and M. Yari, “On the exergoeconomic assessment of employing Kalina cycle for GT-MHR waste heat utilization,” *Energy Convers. Manag.*, vol. 90, pp. 364–374, 2015, doi: <https://doi.org/10.1016/j.enconman.2014.11.039>.
- [57] M. Puig-Arnavat, J. C. Bruno, and A. Coronas, “Modeling of trigeneration configurations based on biomass gasification and comparison of performance,” *Appl. Energy*, vol. 114, pp. 845–856, 2014, doi: 10.1016/j.apenergy.2013.09.013.
- [58] D. S. Ayou and V. Eveloy, “Energy, exergy and exergoeconomic analysis of an ultra low-grade heat-driven ammonia-water combined absorption power-cooling cycle for district space cooling, sub-zero refrigeration, power and LNG regasification,” *Energy Convers. Manag.*, vol. 213, no. August 2019, p. 112790, 2020, doi: 10.1016/j.enconman.2020.112790.
- [59] S. Ogriseck, “Integration of Kalina cycle in a combined heat and power plant, a case study,” *Appl. Therm. Eng.*, vol. 29, no. 14, pp. 2843–2848, 2009, doi: <https://doi.org/10.1016/j.applthermaleng.2009.02.006>.
- [60] S. Vijayaraghavan and Y. Goswami, “On Evaluating Efficiency of a Combined Power and Cooling,” *J. Energy Resour. Technol.*, vol. 125, pp. 221–227, 2003, doi: 10.1115/1.1595110.
- [61] S. Braccio, A. Arteconi, H. T. Phan, N. Tauveron, and N. Le Pierrès, “Energy and exergy analysis of a pilot plant for the combined production of cooling and electricity from a low temperature heat source through an absorption process.,” in *Proceedings of ECOS 2022*, 2022, pp. 529–540.
- [62] N. Lior and N. Zhang, “Energy, exergy, and Second Law performance criteria,” *Energy*, vol. 32, no. 4, pp. 281–296, 2007, doi: 10.1016/j.energy.2006.01.019.
- [63] J. Muye, D. S. Ayou, R. Saravanan, and A. Coronas, “Performance study of a solar absorption power-cooling system,” *Appl. Therm. Eng.*, vol. 97, pp. 59–67, 2016, doi: 10.1016/j.applthermaleng.2015.09.034.
- [64] B. B. Kanbur, L. Xiang, S. Dubey, F. H. Choo, and F. Duan, “Thermoeconomic and environmental assessments of a combined cycle for the small scale LNG cold utilization,” *Appl. Energy*, vol. 204, pp. 1148–1162, 2017, doi: 10.1016/j.apenergy.2017.01.061.
- [65] “The Chemical Engineering Plant Cost Index,” *Chemical Engineering*. Aug. 04, 2022. [Online].

- Available: <https://www.chemengonline.com/pci-home/>
- [66] R. Turton, R. C. Bailie, and W. B. Whiting, *Analysis, Synthesis, and Design of Chemical Processes*. Pearson Prentice Hall, 2012. [Online]. Available: <https://books.google.fr/books?id=f6sbYJuFSycC>
- [67] M. Taal, I. Bulatov, J. Klemeš, and P. Stehlík, “Cost estimation and energy price forecasts for economic evaluation of retrofit projects,” *Appl. Therm. Eng.*, vol. 23, no. 14, pp. 1819–1835, 2003, doi: 10.1016/S1359-4311(03)00136-4.
- [68] S. Lemmens, “Cost engineering techniques & their applicability for cost estimation of organic rankine cycle systems,” *Energies*, vol. 9, no. 7, 2016, doi: 10.3390/en9070485.
- [69] G. Lillo, R. Mastrullo, A. W. Mauro, R. Trinchieri, and L. Viscito, “Thermo-economic analysis of a hybrid ejector refrigerating system based on a low grade heat source,” *Energies*, vol. 13, no. 3, 2020, doi: 10.3390/en13030562.
- [70] S. Quoilin, M. Van Den Broek, S. Declaye, P. Dewallef, and V. Lemort, “Techno-economic survey of organic rankine cycle (ORC) systems,” *Renew. Sustain. Energy Rev.*, vol. 22, pp. 168–186, 2013, doi: 10.1016/j.rser.2013.01.028.
- [71] S. Quoilin, S. Declaye, B. F. Tchanche, and V. Lemort, “Thermo-economic optimization of waste heat recovery Organic Rankine Cycles,” *Appl. Therm. Eng.*, vol. 31, no. 14–15, pp. 2885–2893, 2011, doi: 10.1016/j.applthermaleng.2011.05.014.
- [72] H. G. Berhane, G. G. Gonzalo, J. Laureano, and B. Dieter, “Design of environmentally conscious absorption cooling systems via multi-objective optimization and life cycle assessment,” *Appl. Energy*, vol. 86, no. 9, pp. 1712–1722, 2009, doi: 10.1016/j.apenergy.2008.11.019.
- [73] J. K. Jensen, W. B. Markussen, L. Reinholdt, and B. Elmegaard, “Exergoeconomic optimization of an ammonia–water hybrid absorption–compression heat pump for heat supply in a spray-drying facility,” *Int. J. Energy Environ. Eng.*, vol. 6, no. 2, pp. 195–211, 2015, doi: 10.1007/s40095-015-0166-0.
- [74] N. Shokati, F. Ranjbar, and M. Yari, “A comparative analysis of rankine and absorption power cycles from exergoeconomic viewpoint,” *Energy Convers. Manag.*, vol. 88, pp. 657–668, 2014, doi: 10.1016/j.enconman.2014.09.015.
- [75] H. Rostamzadeh, M. Ebadollahi, H. Ghaebi, and A. Shokri, “Comparative study of two novel micro-CCHP systems based on organic Rankine cycle and Kalina cycle,” *Energy Convers. Manag.*, vol. 183, no. July 2018, pp. 210–229, 2019, doi: 10.1016/j.enconman.2019.01.003.
- [76] S. Klein and G. Nellis, *Mastering EES*. F-Chart, 2014. [Online]. Available: <https://fchart.com/ees/mastering-ees.php>
- [77] H. Ghaebi, T. Parikhani, H. Rostamzadeh, and B. Farhang, “Proposal and assessment of a novel geothermal combined cooling and power cycle based on Kalina and ejector refrigeration cycles,” *Appl. Therm. Eng.*, vol. 130, pp. 767–781, 2018, doi: <https://doi.org/10.1016/j.applthermaleng.2017.11.067>.